Atmospheric Environment 81 (2013) 230–244

Contents lists available at ScienceDirect

Atmospheric Environment

journal homepage: www.elsevier.com/locate/atmosenv

Effects of chemical aging on global secondary organic aerosol using the volatility basis set approach

D.S. Jo [a], R.J. Park [a, *], M.J. Kim [a], D.V. Spracklen [b]

[a] Atmospheric Chemistry Modeling Group, School of Earth and Environmental Science, Seoul National University, Seoul 151-747, Republic of Korea
[b] School of Earth and Environment, University of Leeds, Leeds LS2 9JT, UK

HIGHLIGHTS

- We examined the effects of chemical aging on secondary organic aerosol (SOA).
- The bias of the model was reduced after considering chemical aging.
- Chemical aging increased total SOA production by 53%, from 26.0 Tg to 39.9 Tg yr^{-1}.
- Chemical aging changed volatility distribution of SOA and reduced lifetime of SOA.
- Direct radiative forcing change due to chemical aging of SOA was −0.07 W m^{-2}.

ARTICLE INFO

Article history:
Received 4 April 2013
Received in revised form
23 August 2013
Accepted 28 August 2013

Keywords:
Secondary organic aerosol
Chemical aging
Volatility distribution
Direct radiative forcing

ABSTRACT

A global 3-D chemical transport model (GEOS-Chem) is used with the volatility basis set (VBS) approach to examine the effects of chemical aging on global secondary organic aerosol (SOA) concentrations and budgets. We present full-year simulations and their comparisons with the global aerosol mass spectrometer (AMS) dataset, the Interagency Monitoring of Protected Visual Environments (IMPROVE) dataset from the United States, the European Monitoring and Evaluation Programme (EMEP) dataset from Europe, and water-soluble organic carbon observation data collected over East Asia. Using different chemical aging constants, we find that the model results with 4×10^{-11} cm^3 $molecule^{-1}$ s^{-1} are in better agreement with all observations relative to the model results with other aging constants, without aging, and with the two-product approach. The model simulations are improved when chemical aging is considered, especially for rural regions. However, the simulations still underestimate observed oxygenated organic aerosol (OOA) in urban areas. Two sensitivity simulations including semi-volatile primary organic aerosol (POA) were conducted. We find that including semi-volatile POA improves the model in terms of the hydrogen-like organic aerosol (HOA) to OOA ratio. However, the total OA concentrations are not improved. The total SOA production is considerably increased by 53%, from 26.0 to 39.9 Tg yr^{-1}, after considering chemical aging, remaining lower than top-down estimates of SOA production. Direct radiative forcing (DRF) increases by −0.07 W m^{-2} due to the chemical aging of SOA, which is comparable to the mean DRF (−0.13 W m^{-2}) of OA from the AeroCom multi-model study. This result indicates considerable global and, more importantly, regional climate implications. For example, the regional DRF change due to chemical aging of SOA in the eastern US is −0.29 W m^{-2}, which is 4 times greater in magnitude than the global mean value.

1. Introduction

Organic aerosol (OA) constitutes significant mass fractions (20%–90%) of total dry fine aerosols in the atmosphere (Zhang et al., 2007) and has adverse effects on human health (Folinsbee, 1993; Pavia et al., 1977) and atmospheric visibility (Eidels-Dubovoi, 2002). OA has also received increasing attention in climate studies because of its negative radiative forcing (RF), which may offset a significant fraction of global warming by greenhouse gases (Ming et al., 2005; Myhre et al., 2009). However, the effect of OA on climate is still unclear because of an incomplete understanding of its sources, chemical formation, and physical and chemical characteristics (Hallquist et al., 2009; Kanakidou et al., 2005). In

* Corresponding author. School of Earth and Environmental Sciences, Seoul National University, Seoul 151 742, Republic of Korea. Tel.: +82 2 880 6715.
E-mail address: rjpark@snu.ac.kr (R.J. Park).

1352-2310/$ – see front matter © 2013 Elsevier Ltd. All rights reserved.
http://dx.doi.org/10.1016/j.atmosenv.2013.08.055

particular, secondary organic aerosols (SOAs), which are produced in the atmosphere from gas-phase precursors, are poorly understood relative to primary organic aerosols (POAs), which are directly emitted from sources.

Global models of OA have shown large discrepancies when compared to the observed values because of the limited capability to simulate SOA. Such simulations poorly represent complex SOA formation in the atmosphere (Heald et al., 2005; Volkamer et al., 2006) and have been primarily based on the gas-particle partitioning of semi-volatile organics (Pankow, 1994a,b), which is typically parameterized in models using two oxidation products (called the two-product approach) developed by Odum et al. (1996). The two-product approach has been found to be sufficient for representing experimentally observed SOA yields in chambers (Chung and Seinfeld, 2002; Griffin et al., 1999).

However, many studies have recently shown that chemical aging reactions in the atmosphere are important (Donahue et al., 2006; Jimenez et al., 2009; Kroll and Seinfeld, 2008) because they can lead to decreases in organic volatility, resulting in increases of SOA mass yields. This photochemical aging, which cannot be properly measured in chemical chambers, may contribute to the very low bias in models that do not simulate chemical aging processes in the atmosphere, especially photochemical aging progresses (Volkamer et al., 2006). The main objective of this study is to examine the effects of chemical aging of SOA on global SOA concentrations and budgets using a global 3-D chemical transport model (GEOS-Chem), with the newly implemented capability to simulate SOA aging.

To efficiently simulate chemical aging in the atmosphere, Donahue et al. (2006) proposed the volatility basis set (VBS) approach, which has been extensively used in regional modeling studies (Lane et al., 2008; Murphy and Pandis, 2009; Robinson et al., 2007; Shrivastava et al., 2008; Tsimpidi et al., 2010). Using the VBS approach, SOA-forming reactions from different parent hydrocarbons can be mapped onto the same set of bins encompassing the range of typical ambient organic aerosol mass concentrations ($\sim$0.1–100 $\mu g\ m^{-3}$). Then, aging reactions can easily be simulated by altering the SOA volatility. The VBS approach has recently been implemented in global models. Farina et al. (2010) first used the Goddard Institute for Space Studies General Circulation Model II (GISS GCM II), a "unified" climate model (4° longitude by 5° latitude with 9 vertical layers), to investigate SOA aging. They found that the OA simulation was in better agreement with the Interagency Monitoring of Protected Visual Environments (IMPROVE) data from the United States. Yu (2011) extended the two-product approach by adding an additional low-volatility tracer with a simple aging step and demonstrated improved SOA simulations, especially in rural areas.

For the simulation of SOA aging processes using the VBS approach, we generally assume that gas-phase semi-volatiles react with OH; the saturation vapor pressures of these semi-volatiles is reduced by one order of magnitude. In this process, an aging constant plays an important role because a high value leads to high mass concentrations of SOA, and vice versa. The aging constant of SOA differs greatly in the literature, ranging from 2.5×10^{-12} cm^3 $molecule^{-1}$ s^{-1} to 4×10^{-11} cm^3 $molecule^{-1}$ s^{-1} (Farina et al., 2010; Jathar et al., 2011; Lane et al., 2008; Murphy and Pandis, 2009, 2010; Shrivastava et al., 2008). Therefore, its use in models results in large uncertainty. Here, we compare the observed and simulated SOA concentrations with different aging constants to provide constraints on the aging constant for the VBS method.

In contrast, POA is traditionally regarded as nonvolatile. However, based on laboratory experiments, Robinson et al. (2007) proposed that POA emissions are semi-volatile. A number of modeling studies have employed semi-volatile POA (Jathar et al., 2011; Murphy and Pandis, 2009; Pye and Seinfeld, 2010; Shrivastava et al., 2008), which resulted in decreased OA mass concentrations over the source regions but increased OA concentrations away from the source regions as a result of enhanced SOA formation from semi-volatile POA transport.

Jathar et al. (2011) added semi-volatile POA emissions and SOA aging to the GISS GCM II and found that this addition did not enhance the model performance compared with the observed OA concentrations. However, the simulated SOA-to-OA ratio was greatly increased, resulting in better agreement with the observed ratio. Pye and Seinfeld (2010) simulated semi-volatile POA using GEOS-Chem and obtained results that were consistent with those of Jathar et al. (2011).

In this study, we implemented the VBS in GEOS-Chem (2° longitude by 2.5° latitude with 47 vertical layers), which is driven by assimilated meteorology (Section 2). We extensively evaluated the model by comparing it with observations from a global aerosol mass spectrometer (AMS) dataset compiled by Zhang et al. (2007) with 10 additional observations compiled by Spracklen et al. (2011), the IMPROVE dataset from the United States (Malm et al., 1994), the European Monitoring and Evaluation Programme (EMEP) dataset from Europe (Yttri et al., 2007), and organic carbon (OC) and water-soluble organic carbon (WSOC) concentration data collected over East Asia (Aggarwal and Kawamura, 2009; Batmunkh et al., 2011; Cho and Park, 2013; Choi et al., 2012; Feng et al., 2006; Li et al., 2010; Miyazaki et al., 2007; Pathak et al., 2011; Pavuluri et al., 2013; F. Zhang et al., 2012a,b; Zhao et al., 2013) (Section 3). Then, we examined the effects of semi-volatile POA aging by conducting sensitivity simulations (Section 4). Based on the simulated results, we analyzed the global sources and burdens of SOA (Section 5). As described below, our results regarding the chemical aging of SOA are in better agreement with global observations than the result obtained with no aging; the simulated SOA concentrations are then used to compute the direct radiative forcing (DRF) of SOA to reveal the global climatic implications (Section 6).

2. Model description

2.1. General description

We use the GEOS-Chem global 3-D chemical transport model (Bey et al., 2001) to examine the effect of chemical aging on global SOA budgets and its climatic implications. The GEOS-Chem model (version 9.1.2, http://acmg.seas.harvard.edu/geos/index.html) uses assimilated meteorological data from the Goddard Earth Observing System (GEOS-5) of the NASA Global Modeling and Assimilation Office (GMAO). The data include winds, convective mass fluxes, temperature, clouds, PBL thickness, humidity, and surface properties. We use a horizontal resolution of 2° latitude by 2.5° longitude and 47 vertical hybrid pressure-sigma levels up to 0.01 hpa and conduct a full-year simulation of aerosol-oxidant chemistry for 2009. Detailed descriptions of gas and aerosol simulations can be found in the literature (Bey et al., 2001; Fu et al., 2008; Hudman et al., 2007; Liao et al., 2007; Park et al., 2006; Pye et al., 2009). Here, we focus mainly on OA species simulations, which are briefly discussed below.

The simulation of POA in GEOS-Chem was described in detail by Park et al. (2003). The model includes two POA tracers: hydrophobic and hydrophilic POAs. Combustion sources emit hydrophobic POA, which then becomes hydrophilic with an e-folding time of 1.15 day (Cooke et al., 1999; Park et al., 2003). We assume that 50% of POAs emitted are hydrophobic (Park et al., 2003). The SOA simulations are discussed in detail in Section 2.2. The simulation of other inorganic salts in GEOS-Chem was described by Park

et al. (2004). Nitrate aerosol formation is calculated using ISORROPIA II (Fountoukis and Nenes, 2007; Pye et al., 2009), which computes the H_2SO_4–HNO_3–NH_3–H_2O thermodynamics.

Wet deposition is simulated using the scheme described by Liu et al. (2001) and applies only to hydrophilic aerosols. This scheme accounts for scavenging in convective updrafts, rainout from convective anvils, and rainout and washout from large-scale precipitation (Mari et al., 2000). Our dry deposition algorithm uses a standard resistance-in-series model dependent on local surface types and meteorological conditions, as described by Wang et al. (1998).

We use global fossil fuel (3.05 TgC yr^{-1}) and biofuel (6.28 TgC yr^{-1}) emissions of POA from Bond et al. (2007), who estimated emissions by country, sector, fuel type, and fuel/technology. Anthropogenic VOC (aromatics: benzene, toluene, and xylene) emissions are obtained from the REanalysis of the TROpospheric chemical composition (RETRO) inventory; the total annual anthropogenic VOC emission is 13.57 TgC yr^{-1}.

For biomass burning emissions, we use the Global Fire Emission Database version 3 (GFEDv3) inventory, which has been widely used in global CTM studies (van der Werf et al., 2010). The global annual biomass-burning POA emission is 13.49 TgC yr^{-1}. Although anthropogenic emissions are a main contributor to global aromatic VOC emissions, biomass burning also slightly contributes to aromatic VOC emissions. The annual biomass-burning emission is 1.86 TgC yr^{-1}, contributing 12% of the total aromatic VOC emissions. We convert the GFEDv3 monthly data from van der Werf et al. (2010) into 3-h resolution data based on the fire fraction information from Mu et al. (2011) who used MODIS-derived measurements of active fires from the Terra and Aqua satellites and active fire observations with the Geostationary Operational Environmental Satellite Wildfire Automated Biomass Burning Algorithm (http://www.globalfiredata.org/Data/index.html).

Biogenic emissions are obtained from the Model of Emissions of Gases and Aerosols from Nature (MEGAN) v2.1 inventory (Guenther et al., 2012). The MEGAN inventory includes isoprene, methylbutenol, and seven monoterpene compounds (α-pinene, β-pinene, limonene, myrcene, sabinene, 3-carene and ocimene). The emissions of these compounds are calculated on the basis of emission activity factors, canopy environment, leaf age, and soil moisture. The global biogenic emissions of isoprene and the seven monoterpenes are 456 TgC yr^{-1} and 91 TgC yr^{-1}, respectively.

2.2. SOA simulation

SOA simulation in GEOS-Chem is based on the scheme developed by Chung and Seinfeld (2002) who used the two-product approach. This scheme has been used in previous studies (Heald et al., 2005; Henze and Seinfeld, 2006; Henze et al., 2008; Liao et al., 2007). A detailed description of the two-product approach in GEOS-Chem can be found in Liao et al. (2007). Here, we briefly discuss a few updates. The model considers nine lumped parent hydrocarbons that consist of monoterpenes, sesquiterpenes, isoprene, and aromatic compounds. Oxidation of these parent hydrocarbons by OH, O_3, and NO_3 yields a total of 56 products. At every model time step, these oxidation products are partitioned into a gas phase (SOG) and a particle phase (SOA), which are determined by equilibrium partitioning coefficients and preexisting POA concentrations. These products are then lumped into 10 tracers (5 for gases and 5 for aerosols). Depending on the source, 8 tracers are biogenic, and 2 are anthropogenic. This scheme does not account for aging of the oxidation products.

In our study, we implemented the VBS approach (Donahue et al., 2006) in GEOS-Chem to consider aging reactions. First, we partitioned all semi-volatile organics by volatility, with 6 bins defined by a set of prescribed vapor pressures as follows: $[C^*_i] = [0.01, 0.1, 1, 10, 100, 1000]$ μg m^{-3} at 300 K. C^*_i is the effective saturation concentration of species i. The temperature dependence of C^* is calculated using the Clausius–Clapeyron equation:

$$C^*_T = C^*_{T_{\mathrm{ref}}} \frac{T_{\mathrm{ref}}}{T} \exp\left[\frac{\Delta H}{R}\left(\frac{1}{T_{\mathrm{ref}}} - \frac{1}{T}\right)\right] \quad (1)$$

where ΔH is the enthalpy of vaporization, and R is the universal gas constant. ΔH is one of the most important parameters for SOA formation because it determines the rate that the saturation vapor pressure decreases with decreasing temperature. A high ΔH value leads to a higher SOA mass increase with decreasing temperatures lower than the reference temperature. The ΔH values differ from study to study, ranging from ~10 kJ mol^{-1} to ~180 kJ mol^{-1} (Yu, 2011). In this study, the ΔH values are assumed to be 100 kJ mol^{-1} for $C^* = 1$ μg m^{-3} and decrease by 6 kJ mol^{-1} for each increase in order of magnitude of C^* (Donahue et al., 2006; Robinson et al., 2007). The GEOS-Chem model previously used 42 kJ mol^{-1} for all SOA tracers (Chung and Seinfeld, 2002).

In the VBS approach, each VOC reacts with OH, O_3, and NO_3; the resulting oxidation products (semi-volatile species) are allocated into 4 bins, $[C^*_i] = [1, 10, 100, 1000]$ μg m^{-3}, using yield parameters based on chamber studies. We adopt the yield parameters compiled by Farina et al. (2010) (Table 1). Following Henze et al. (2008), we consider one NO_x level (low NO_x) for biogenic species and two NO_x levels (high and low NO_x) for aromatic species.

Compared with previous SOA studies using GEOS-Chem, we have considerably updated the yield parameters of semi-volatile species, as shown in Table 1. For example, the isoprene yield parameter of the VBS is 0.04, based on several chamber studies (Farina et al., 2010; Dommen et al., 2006; Kleindienst et al., 2007; Kroll et al., 2005, 2006). However, the parameter for the two-product approach is 0.26 (Henze and Seinfeld, 2006; Kroll et al., 2006), which is much higher. Yield parameters of other VOCs also differ between the VBS and the two-product schemes. For example, we use 0.52–0.79 for aromatic VOCs with the VBS approach, which are higher than the values (0.09–0.47) used by Henze et al. (2008). The effects of the updated yield parameters on the global budget of SOA are discussed in Section 5.

The chemical aging of semi-volatile organics is accounted for by decreasing their saturation vapor pressures. In our study, we only

Table 1
Yield parameters used in this study (Farina et al., 2010). High-NO_x yields are presented in parentheses. Aromatic yields are scaled with the RO_2/VOC ratio because GEOS-Chem applies yield parameters to RO_2 (Henze et al., 2008).

Oxidants	Species[a]	Saturation concentration (μg m^{-3})			
		1	10	100	1000
OH and O_3	ALPH	0.07	0.06	0.24	0.41
	LIMO	0.32	0.31	0.3	0.6
	TERP	0.01	0	0.54	0
	ALCO	0.03	0.06	0.1	0.5
	SESQ	0	0.55	0.54	0
	ISOP	0.02	0.02	0	0
	BENZ	0.0049 (0.0049)	0.1079 (0.1079)	0.2600 (0.1521)	0.3140 (0.2600)
	TOLU	0.0053 (0.0053)	0.1170 (0.1170)	0.2818 (0.1649)	0.3403 (0.2818)
	XYLE	0.0057 (0.0057)	0.1247 (0.1247)	0.3004 (0.1757)	0.3628 (0.3004)
NO_3	Monoterpenes	0.07	0.06	0.24	0.41
	Sesquiterpenes	0.07	0.06	0.24	0.41

[a] ALPH – pinene, sabinene, carene, and terpenoid ketones; LIMO – limonene; TERP – terpinene and terpinolene; ALCO – myrcene, terpenoid alcohols and ocimene; SESQ – sesquiterpenes; ISOP – isoprene; BENZ – benzene; TOLU – toluene; XYLE – xylene.

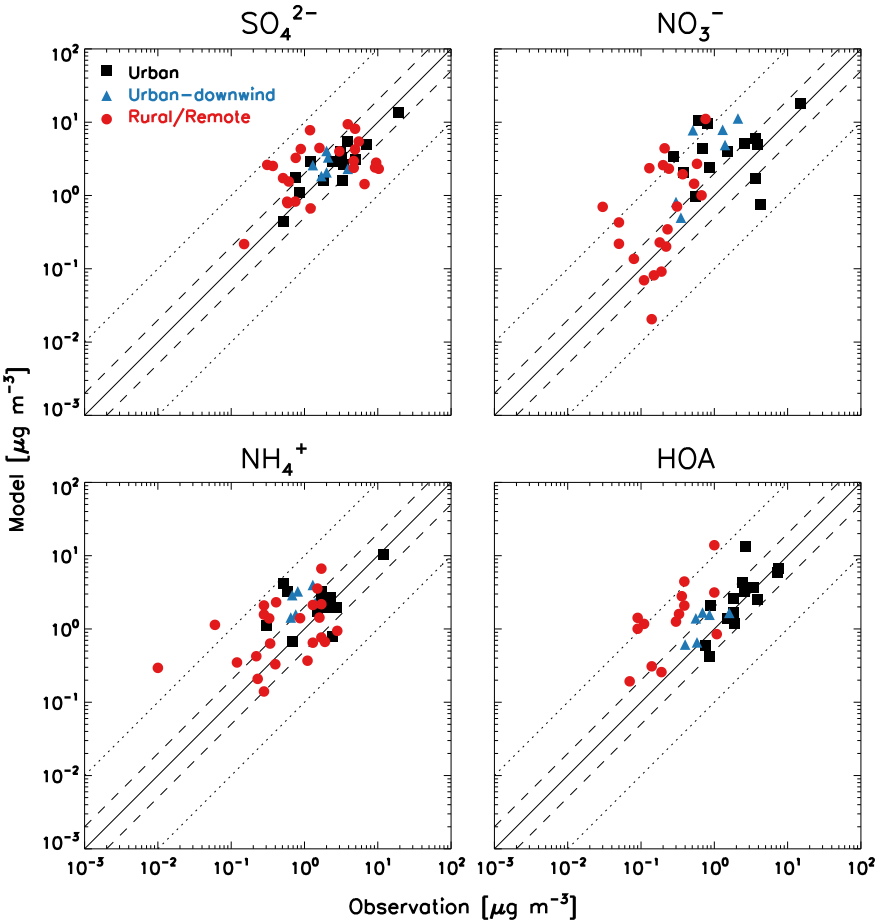

Fig. 1. Scatter plots of the modeled (y-axis) versus observed (x-axis) SO_4^{2-}, NO_3^-, NH_4^+, and HOA. We multiplied the carbon mass of OA by 2.1 to account for the non-carbon mass. We excluded the observed HOA reported as 0.00 μg m^{-3}. Information on the AMS observation sites is given in Zhang et al. (2007) and Spracklen et al. (2011). The 1:1 line (solid), 2:1 lines (dashed), and 10:1 lines (dotted) are indicated.

applied the aging to aromatic species. Biogenic species are not aged following previous global modeling studies (Farina et al., 2010; Jathar et al., 2011). Lane et al. (2008) and Murphy and Pandis (2009) found that models overestimated the observed OA concentrations when they considered the aging of both biogenic and anthropogenic SOA. Murphy and Pandis (2010) further investigated SOA aging and found that including only anthropogenic SOA aging resulted in the best agreement with observations relative to the other cases, which used only biogenic SOA aging, no aging, and both biogenic and anthropogenic SOA aging.

There may be two reasons related to biogenic SOA aging for the overestimation of OA concentrations in models. First, mass yield parameters of biogenic SOA represent completed reactions; hence, they do not need to be aged (i.e., biogenic SOA aging is already accounted for in the yield parameters) (Farina et al., 2010; Jathar et al., 2011). This can be partially explained from chamber studies – the growth of SOA from VOCs having one double bond stops once all the VOCs are consumed (i.e., no aging process); some biogenic VOCs (e.g., α-pinene, β-pinene, Δ^3-carene) have one double bond (Ng et al., 2006). These monoterpenes constitute a large portion of biogenic SOA (Hallquist et al., 2009). Second, the chemical aging using the VBS approach only accounts for functionalization. However, in the real atmosphere, there might be an offset between functionalization (decreased volatility) and fragmentation (increased volatility) effects, especially for biogenic SOA (Murphy et al., 2012).

At every time step, we calculate the amount of aged gas-phase aromatic SOAs proportional to the reaction with OH using various rate constants: 1×10^{-10}, 4×10^{-11}, 1×10^{-11}, 4×10^{-12}, and 1×10^{-12} cm^3 molecule^{-1} s^{-1}. The vapor pressure of these aged SOAs is reduced by one order of magnitude, and they are moved into the next lower bin (Jathar et al., 2011). Additionally, we further conduct a no aging case with the VBS and the two-product schemes as a control run. All SOAs in the model are assumed to be hydrophilic aerosols, which are subject to wet deposition.

3. Model evaluation

We focused our model evaluation on surface networks of OA observations. First, we compared the model with the global AMS dataset, which measures OA into two categories: hydrocarbon-like OA (HOA) and oxygenated OA (OOA). We also used two regional observation network datasets, IMPROVE and EMEP, from the United States and Europe, respectively. These data do not classify OA, as in the AMS dataset, and instead provide total OC concentrations that we used for comparison with the model simulations. Finally, we evaluated the model in East Asia using OC and WSOC data collected over East Asia.

3.1. Global

We used the AMS dataset compiled by Zhang et al. (2007) along with 10 more observations compiled by Spracklen et al. (2011) to evaluate our global simulations, which were conducted for 2009. The simulated year is different from the observation

Table 2
Statistical parameters for the evaluation of inorganic aerosols and HOA against AMS observations. Regressions were computed using the reduced-major-axis method (Hirsch and Gilroy, 1984).

Type	Species	Data points	Slope	R	NMB	NME	RMSE
Urban	SO_4^{2-}	14	0.68	0.95	−0.11	0.33	1.89
	NO_3^-	14	1.23	0.67	0.90	1.19	4.24
	NH_4^+	14	0.81	0.86	0.21	0.48	1.5
	HOA	14	1.59	0.49	0.26	0.52	2.97
Urban downwind	SO_4^{2-}	6	−0.93	−0.09	0.24	0.49	1.28
	NO_3^-	6	5.91	0.79	4.55	4.55	5.66
	NH_4^+	6	3.02	0.43	1.75	1.75	1.83
	HOA	6	1.15	0.61	0.61	0.61	0.61
Rural	SO_4^{2-}	24	0.76	0.16	0.00	0.84	3.62
	NO_3^-	23	11.71	0.63	4.87	5.06	2.54
	NH_4^+	23	1.87	0.33	0.55	1.12	1.44
	HOA	14	9.7	0.56	5.22	5.30	3.8
All	SO_4^{2-}	44	0.72	0.57	−0.02	0.61	2.91
	NO_3^-	43	1.64	0.63	1.78	2.02	3.71
	NH_4^+	43	1.01	0.71	0.48	0.82	1.52
	HOA	34	1.78	0.43	0.85	1.07	3.11

period of the AMS dataset (2000–2008). However, this difference is not significant in terms of monthly variations (on which our model evaluation is primarily focused), as shown in previous studies (Farina et al., 2010; Jathar et al., 2011; Spracklen et al., 2011; Yu, 2011).

The AMS combines aerodynamic lens inlet technology with thermal vaporization and electron-impact mass spectrometry to provide measurements of speciated PM mass concentrations and size distributions. Canagaratna et al. (2007) described AMS measurement techniques and associated issues in detail. Factor analysis of AMS spectra can be used to divide OA into two groups: HOA and OOA. On the basis of many recent observations (Aiken, 2009; Aiken et al., 2008; Dzepina et al., 2009; Lanz et al., 2007; Zhang et al., 2005), we assumed that POA is equivalent to the observed HOA and that SOA is equivalent to the observed OOA.

Fig. 1 shows the scatter plots of the simulated concentrations versus the observed concentrations for SO_4^{2-}, NO_3^-, NH_4^+ and HOA (POA). A global comparison of inorganic SO_4^{2-}, NO_3^- and NH_4^+ aerosols provides an evaluation of the GEOS-Chem aerosol simulations in terms of transport and other depositional loss processes (Park et al., 2004). The statistical parameters, including the regression slope, correlation coefficient (R), normalized mean bias (NMB), normalized mean error (NME) and root mean square error (RMSE), between the observations and the model are summarized in Table 2. We found that the SO_4^{2-} and NH_4^+ concentrations are generally in good agreement with the observations (NMBs are −2% and 48%, respectively), but the NO_3^- concentrations are overestimated (NMB is 178%) in the model. This overestimation occurs mainly in Europe (NMB is 521%) where other inorganic SO_4^{2-} and NH_4^+ aerosols are also overestimated. The NMB of SO_4^{2-} is 46% and the NMB of NH_4^+ is 220%. This result is most likely due to the overestimated regional EMEP emission inventories in Europe. Overall, the model reproduced the inorganic concentrations well

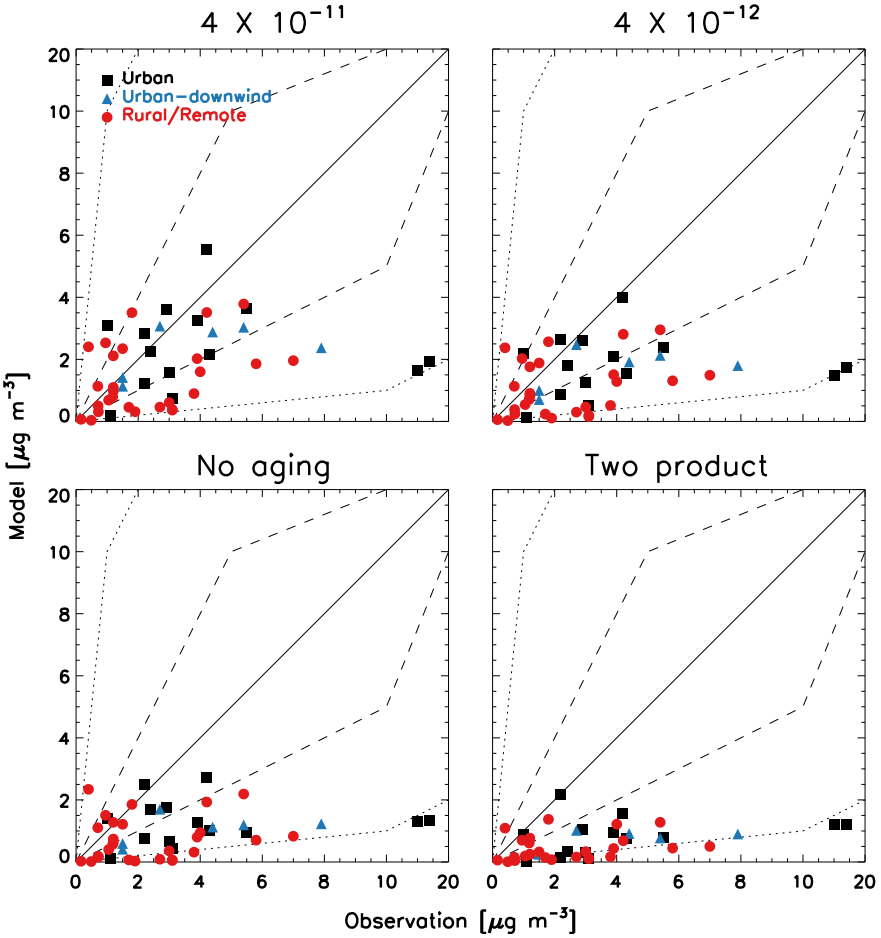

Fig. 2. Scatter plots of the modeled (y-axis) versus observed (x-axis) OOA for selected cases, i.e., the VBS approach with aging constants of 4×10^{-11} and 4×10^{-12} cm^3 molecule^{-1} s^{-1}, the VBS approach with no aging condition, and the two-product scheme. The 1:1 line (solid), 2:1 lines (dashed), and 10:1 lines (dotted) are indicated.

except for NO_3^- concentrations, similar to previous GEOS-Chem evaluations conducted in East Asia (Jeong et al., 2010) and in the United States (Heald et al., 2012).

Because GEOS-Chem transports organic carbon (OC) mass as a tracer for POA, we needed to convert the carbon mass of POA (POC) into the organic matter concentrations for the comparison with the AMS observations, which were provided as organic matter (OM) mass concentrations. For the conversion of POC into POM, we multiplied the model POC concentrations by an OM/OC ratio of 2.1, following the method used in previous studies with GEOS-Chem (Henze et al., 2008; Pye et al., 2010; Pye and Seinfeld, 2010). Moreover, the model transports organic matter mass for SOA. Therefore, we did not need to apply the OM/OC ratio to SOA tracers. Fig. 1 shows that the model overestimated the globally observed HOA (POA) concentrations; the NMB is 85%. It should be noted that NMBs were not significantly high in urban (26%) and urban downwind (61%) regions. The overestimation results primarily from rural regions (522%), where very low HOA concentrations were observed (this overestimation still exists if we had applied a different OM/OC ratio, e.g., 1.4 (314%) and 1.6 (374%)). High bias in regions away from the source region implies that POA loss processes were missed in the model, especially in rural areas. Treating POA as semi-volatile rather than non-volatile species may reduce this discrepancy. This is discussed in Section 4.

Fig. 2 compares the model results with the AMS observations of OOA (SOA) for selected cases, i.e., the VBS approach with aging constants of 4×10^{-11} and 4×10^{-12} cm^3 $molecule^{-1}$ s^{-1}, the VBS approach with no aging, and the two-product scheme. The statistical parameters for all cases are presented in Table 3. First, the VBS with no aging yielded slightly lower RMSE and NME values than the two-product method because of the updated yield parameters. The simulated results that include aging are in better agreement with the observations than the simulations performed with no aging and the two-product scheme. The model performance improved with an increase in the aging constant, i.e., lowered RMSE and NME, and increased R (Table 3). However, the model improvement was saturated beyond 4.0×10^{-11} cm^3 $molecule^{-1}$ s^{-1} because no significant differences were found in simulated results using the highest aging constant (i.e., 1×10^{-10} cm^3 $molecule^{-1}$ s^{-1}).

In urban downwind and rural regions, R increased as the aging effect increased. This implies that aging reactions become significant as the photochemical aging time increases in the atmosphere. However, in urban regions, R decreased as the aging effect increased and became much lower than the R values in other regions. This result suggests that OOA concentrations in urban regions are significantly affected by local sources, which are subgrid-scale processes in our model because the spatial resolution ($2^\circ \times 2.5^\circ$) was too coarse to capture these sources. In contrast, in remote regions, grid-scale processes are more important. Therefore, the model reproduced the observed OOA concentrations relatively well in these locales.

By comparing OOA between the two-product scheme and the VBS approach with no aging, we found that the R values for the two-product scheme were higher than those for the VBS approach with no aging, indicating that the former was more successful at reproducing the observed variability even though the RMSE of the two-product scheme was higher than that of the VBS approach with no aging. Because neither method considers chemical aging of SOA, the difference in R between the simulations resulted primarily from the yield parameters, which should be investigated further to improve global models.

For total OA (TOA), the model is similar to that of OOA except that the R values are nearly equivalent. In summary, chemical aging reduces the low biases of the modeled OOA (from −71% to −43%) and TOA (from −29% to −8%), and its effect became more important farther away from the sources (i.e., R increased from urban to the rural regions, as shown in Table 3).

Table 3
Statistical parameters for the evaluation of OOA and TOA against AMS observations. The numbers of data points are given in parentheses.

Type	Case	OOA					TOA				
		Slope	R	NMB	NME	RMSE	Slope	R	NMB	NME	RMSE
Urban (14)	1×10^{-10}	−0.29	−0.08	−0.48	0.64	5.53	0.55	0.30	−0.21	0.58	6.75
	4×10^{-11}	−0.28	−0.06	−0.50	0.64	5.54	0.55	0.30	−0.22	0.58	6.75
	1×10^{-11}	−0.24	−0.01	−0.57	0.66	5.60	0.55	0.32	−0.27	0.58	6.77
	4×10^{-12}	0.20	0.02	−0.63	0.68	5.68	0.55	0.34	−0.30	0.59	6.81
	1×10^{-12}	0.16	0.06	−0.70	0.73	5.81	0.55	0.35	−0.34	0.61	6.90
	No aging	0.15	0.06	−0.74	0.76	5.92	0.55	0.35	−0.37	0.63	6.98
	Two product	0.12	0.31	−0.83	0.83	6.09	0.56	0.38	−0.43	0.65	7.05
Urban downwind (6)	1×10^{-10}	0.35	0.53	−0.38	0.42	2.46	0.28	0.46	−0.21	0.40	2.50
	4×10^{-11}	0.34	0.53	−0.41	0.44	2.54	0.28	0.45	−0.24	0.41	2.55
	1×10^{-11}	0.30	0.52	−0.49	0.50	2.79	0.27	0.40	−0.31	0.43	2.76
	4×10^{-12}	0.27	0.50	−0.57	0.57	3.03	0.26	0.35	−0.37	0.45	2.96
	1×10^{-12}	0.23	0.48	−0.67	0.67	3.34	0.26	0.29	−0.45	0.48	3.22
	No aging	0.19	0.48	−0.73	0.73	3.56	0.24	0.25	−0.51	0.51	3.42
	Two product	0.14	0.65	−0.82	0.82	3.84	0.20	0.31	−0.58	0.58	3.66
Rural (27)	1×10^{-10}	0.63	0.39	−0.39	0.64	1.93	1.51	0.55	0.18	0.64	2.57
	4×10^{-11}	0.61	0.38	−0.42	0.65	1.96	1.51	0.55	0.16	0.64	2.55
	1×10^{-11}	0.55	0.34	−0.48	0.68	2.05	1.48	0.53	0.10	0.65	2.53
	4×10^{-12}	0.50	0.30	−0.54	0.71	2.15	1.45	0.51	0.04	0.65	2.52
	1×10^{-12}	0.43	0.22	−0.62	0.74	2.30	1.42	0.49	−0.03	0.65	2.53
	No aging	0.39	0.15	−0.68	0.77	2.40	1.40	0.47	−0.08	0.65	2.54
	Two product	0.22	0.28	−0.82	0.84	2.56	1.42	0.47	−0.21	0.65	2.63
All (47)	1×10^{-10}	0.40	0.24	−0.43	0.61	3.47	0.72	0.47	−0.08	0.58	4.26
	4×10^{-11}	0.38	0.25	−0.45	0.62	3.49	0.72	0.47	−0.10	0.58	4.26
	1×10^{-11}	0.34	0.26	−0.52	0.64	3.57	0.70	0.47	−0.15	0.58	4.28
	4×10^{-12}	0.29	0.26	−0.58	0.67	3.66	0.69	0.46	−0.20	0.59	4.31
	1×10^{-12}	0.25	0.24	−0.66	0.72	3.81	0.68	0.46	−0.25	0.61	4.38
	No aging	0.22	0.22	−0.71	0.76	3.92	0.68	0.45	−0.29	0.62	4.44
	Two product	0.15	0.40	−0.82	0.83	4.08	0.68	0.46	−0.38	0.64	4.53

3.2. United States

We used observations from the IMPROVE network for 1988–2012 to evaluate the model in the United States (Malm et al., 1994). Most of the sites are situated in rural regions measuring background concentrations of OA. The number of sites increased from 37 in 1988 to 219 in 2012. The data were observed every 3 days; more than 280,000 samples were used for our comparison. However, the IMPROVE network does not separate HOA and OOA and instead provides total OC concentrations, which are measured using the thermal optical reflectance (TOR) method (Chow et al., 1993). For comparison with the model results, we computed the observed monthly mean concentrations averaged on the $2^\circ \times 2.5^\circ$ model grid.

Fig. 3 shows the scatter plots of the simulated versus observed OC concentrations, and the statistics are given in Table 4. The model with a high aging constant showed improved results; less scatter was found and the NMB was reduced from −30% to 2%. The *R* value also improved as the aging constant increased. We found that the NME slightly increased with the 1×10^{-10} (0.43) and 4×10^{-11} (0.42) cm^3 $molecule^{-1}$ s^{-1} aging constants. However, these simulations are still better than those using either the two-product scheme (0.56) or the no aging cases (0.47). Statistical parameters show that the VBS approach with chemical aging is better than the other methods for reproducing the observations in the United States.

3.3. Europe

Fig. 4 shows the comparison of the model results with monthly mean observations of OC at EMEP sites for 2002–2003 (Yttri et al., 2007). The EMEP also provides total OC concentrations, which were measured using the thermal optical transmittance (TOT) method (Birch and Cary, 1996).

Similar to the comparison with the United States, including chemical aging reduces biases and errors in the model simulations (Table 4). However, in contrast to the IMPROVE comparison, *R* remained unchanged, and the model continued to underestimate OC concentrations. The model appears to be better in the United States than Europe because IMPROVE sites in the United States are primarily situated in rural areas. The mean OC concentration from IMPROVE is 1.19 μgC m^{-3}, three times lower than the OC concentration from EMEP (3.83 μgC m^{-3}). As discussed in Section 3.1, the model reproduced observations well in downwind and rural areas, where grid-scale processes are dominant.

3.4. East Asia

Long-term observations of OA in East Asia are unavailable. Instead, we collected episodic OC and WSOC data measured on relatively short-term periods from the literature (Table S1). For the evaluation of SOA in the model, we used observed WSOC concentrations, which can be used as a proxy for SOA (Sullivan et al., 2006;

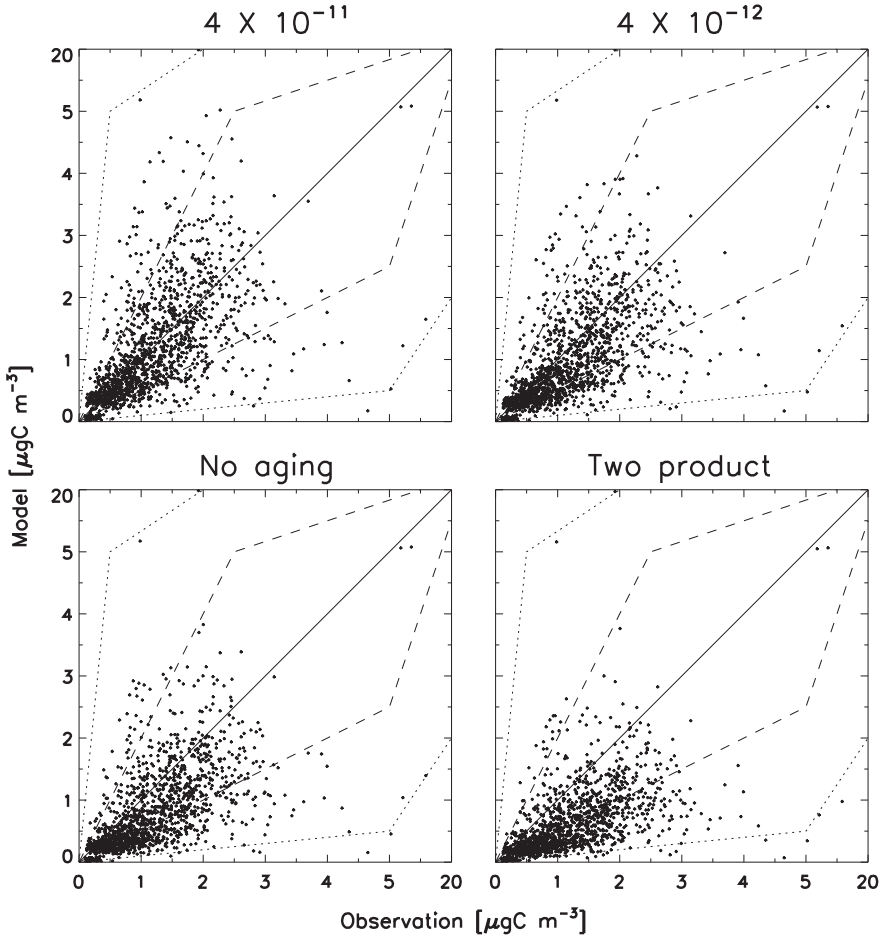

Fig. 3. Scatter plots of OC concentrations between IMPROVE observations (*x*-axis) and the model (*y*-axis) for selected cases, i.e., the VBS approach with aging constants of 4×10^{-11} and 4×10^{-12} cm^3 $molecule^{-1}$ s^{-1}, the VBS approach with no aging condition, and the two-product scheme. The 1:1 line (solid), 2:1 lines (dashed), and 10:1 lines (dotted) are indicated. The number of points is 1441.

Table 4
Statistical parameters for the evaluation of OC against IMPROVE and EMEP observations.

Case	IMPROVE OC					EMEP OC				
	Slope	*R*	NMB	NME	RMSE	Slope	*R*	NMB	NME	RMSE
1×10^{-10}	1.20	0.50	0.02	0.43	0.97	0.47	0.27	−0.42	0.53	3.05
4×10^{-11}	1.17	0.50	−0.02	0.42	0.96	0.47	0.27	−0.44	0.54	3.10
1×10^{-11}	1.11	0.49	−0.10	0.41	0.94	0.45	0.26	−0.48	0.56	3.19
4×10^{-12}	1.06	0.48	−0.17	0.42	0.93	0.44	0.26	−0.51	0.58	3.26
1×10^{-12}	1.02	0.47	−0.25	0.44	0.95	0.44	0.27	−0.55	0.61	3.34
No aging	0.99	0.46	−0.30	0.47	0.97	0.43	0.28	−0.58	0.63	3.39
Two product	0.87	0.42	−0.47	0.56	1.05	0.34	0.28	−0.68	0.70	3.65

Weber et al., 2007). However, WSOC concentrations are not entirely SOA in the atmosphere because some POA species, especially those from biomass burning, may be soluble (Sullivan et al., 2006, 2004; Weber et al., 2007). Therefore, the observed WSOC concentrations should be regarded as the upper limit of SOA concentrations. However, the annual biomass-burning contribution to OC is relatively minor in East Asia (Jeong et al., 2010). We also compared the observed and simulated OC concentrations in East Asia as an alternative validation of the model.

Fig. 5 displays a comparison of the simulated and observed WSOC concentrations over East Asia. The statistical parameters of the OC and WSOC comparison are listed in Table 5. We found that the model underestimated the observed WSOC (NMB: −84% to −70%) and OC (NMB: −70% to −60%) regardless of the chemical aging constant used. This underestimation resulted because the observations in East Asia were mainly from highly polluted urban regions (e.g., Beijing and Guangzhou) and resolution of the model is too coarse to simulate the high concentrations from heavily polluted megacities – the observed mean concentration of OC is 14.19 μgC m^{-3} and that of WSOC is 4.16 μgC m^{-3}. The observed mean WSOC concentration over East Asia is even higher than the mean OC concentration from IMPROVE (1.19 μgC m^{-3}) and EMEP (3.83 μgC m^{-3}). Second, although there are slight improvements in the statistical parameters (NME from 84 to 71% and RMSE from 4.16 to 3.66 μgC m^{-3}) after the inclusion of chemical aging, they are very limited. The model still shows significant low biases with the

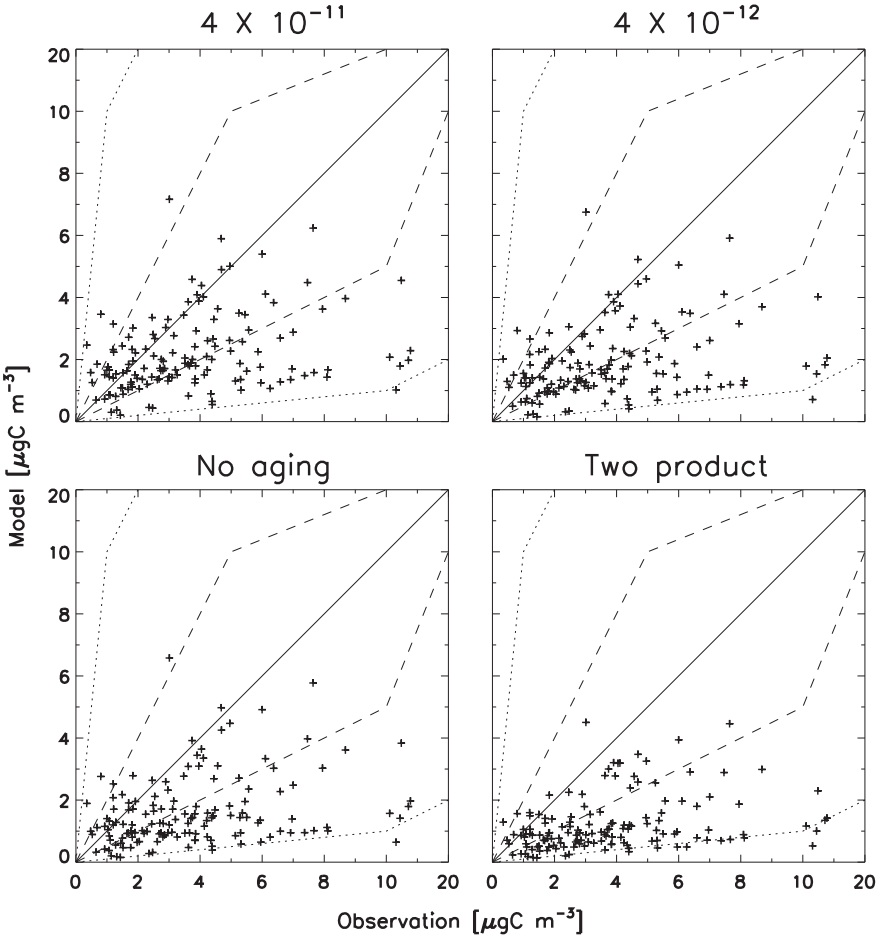

Fig. 4. Scatter plots of OC concentrations between EMEP observations (*x*-axis) and the model (*y*-axis) for selected cases, i.e., the VBS approach with aging constants of 4×10^{-11} and 4×10^{-12} cm^3 $molecule^{-1}$ s^{-1}, the VBS approach with no aging condition, and the two-product scheme. The 1:1 line (solid), 2:1 lines (dashed), and 10:1 lines (dotted) are indicated. The number of points is 142.

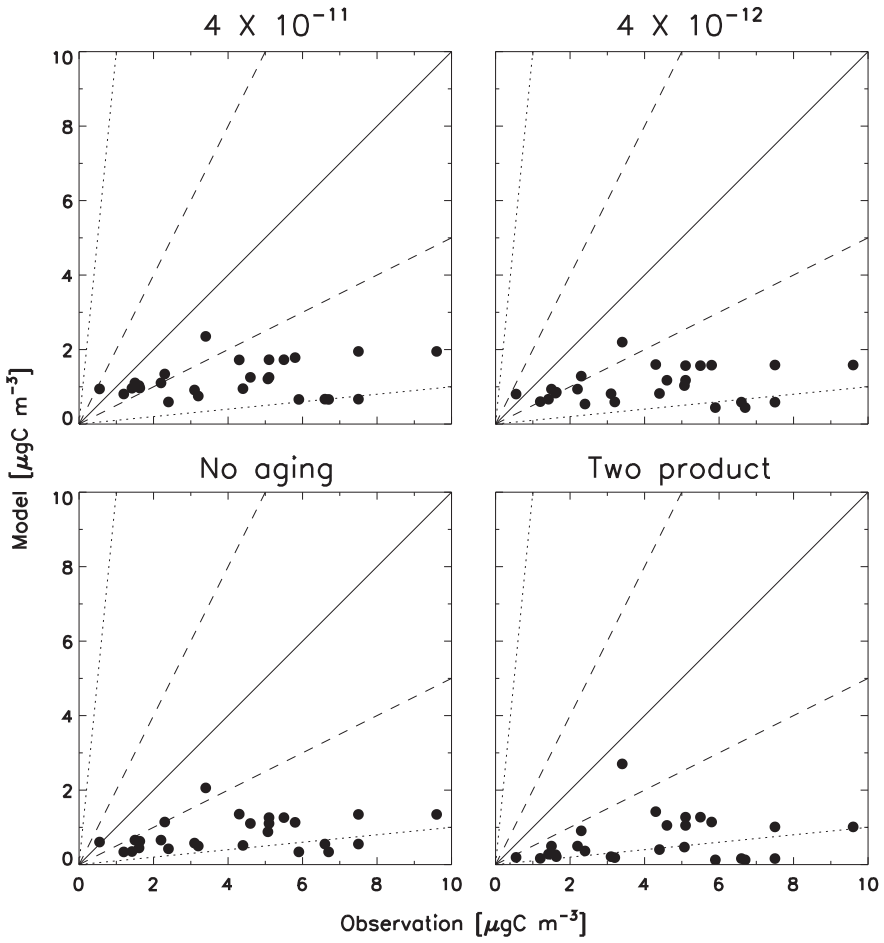

Fig. 5. Scatter plots of WSOC concentrations between observations (*x*-axis) and the model (*y*-axis) over East Asia for selected cases, i.e., the VBS approach with aging constants of 4×10^{-11} and 4×10^{-12} cm^3 $molecule^{-1}$ s^{-1}, the VBS approach with no aging condition, and the two-product scheme. The 1:1 line (solid), 2:1 lines (dashed), and 10:1 lines (dotted) are indicated. The number of points is 27 and associated references are given in Table S1.

highest aging constant, indicating the possibility of missing sources of SOA in East Asia (Liu et al., 2012).

3.5. Discussion

In the evaluations above, the VBS approach with chemical aging showed better agreement with the observations in terms of mean mass concentrations (NMB) and errors (NME and RMSE). However, the model performance differs regionally. In polluted urban regions, the model significantly underestimates the observed OA, and *R* is also low. In clean rural areas, the model reproduces the observed OA with high *R* values and small biases.

Comparisons between the observations and the model results with different aging constants allowed us to provide a constraint on the aging constants for the VBS approach. We found that the simulation using 4×10^{-11} cm^3 $molecule^{-1}$ s^{-1} agreed best with the global SOA observations despite significant biases in some regions. The model with the highest aging constant, i.e., 1×10^{-10} cm^3 $molecule^{-1}$ s^{-1}, exhibited a similar performance, and less improvement was observed in some regions compared to simulations using 4×10^{-11} cm^3 $molecule^{-1}$ s^{-1}. Furthermore, the 1×10^{-10} cm^3 $molecule^{-1}$ s^{-1} aging constant has never been used in previous studies because it is too high. Therefore, we recommend the use of 4×10^{-11} cm^3 $molecule^{-1}$ s^{-1} with the VBS approach. All of the results below are from the model with this value, including a semi-volatile POA simulation, global budget analysis, and DRF estimation.

Although the use of chemical aging reduced the gap between the model and the observations, the model still underestimated the

Table 5
Statistical parameters for the comparison between the simulated and the observed OC and WSOC in East Asia. The number of observation points is given in parentheses.

Case	OC (57)					WSOC (27)				
	Slope	*R*	NMB	NME	RMSE	Slope	*R*	NMB	NME	RMSE
1×10^{-10}	0.27	0.63	−0.66	0.66	12.35	0.21	0.31	−0.70	0.71	3.66
4×10^{-11}	0.27	0.63	−0.66	0.66	12.38	0.21	0.29	−0.71	0.72	3.69
1×10^{-11}	0.27	0.63	−0.66	0.67	12.45	0.20	0.26	−0.73	0.74	3.78
4×10^{-12}	0.27	0.63	−0.67	0.68	12.50	0.20	0.25	−0.75	0.76	3.84
1×10^{-12}	0.27	0.63	−0.68	0.68	12.58	0.19	0.28	−0.78	0.78	3.92
No aging	0.27	0.64	−0.68	0.69	12.63	0.19	0.32	−0.80	0.80	3.99
Two product	0.27	0.62	−0.70	0.70	12.82	0.26	0.20	−0.84	0.84	4.16

Table 6
Statistical parameters from the comparison between the semi-volatile POA simulation and the AMS observations.

Type	Species	With the VBS approach					Simple conversion				
		Slope	*R*	NMB	NME	RMSE	Slope	*R*	NMB	NME	RMSE
Urban	HOA	0.32	0.37	−0.75	0.75	2.82	0.72	0.44	−0.42	0.59	2.24
	OOA	0.5	0.28	−0.20	0.63	4.74	0.43	0.23	−0.22	0.63	4.81
	TOA	0.42	0.3	−0.40	0.59	7.08	0.48	0.3	−0.29	0.58	6.84
Urban downwind	HOA	0.37	0.33	−0.72	0.72	0.67	0.7	0.54	−0.30	0.37	0.41
	OOA	0.42	0.48	−0.23	0.40	2.2	0.38	0.53	−0.27	0.40	2.24
	TOA	0.39	0.38	−0.31	0.42	2.75	0.29	0.46	−0.28	0.39	2.63
Rural	HOA	1.38	0.46	−0.20	0.77	0.45	3.7	0.54	0.80	1.35	1.18
	OOA	1.36	0.64	0.18	0.57	1.92	1.11	0.61	0.04	0.54	1.68
	TOA	1.37	0.65	0.16	0.59	2.12	1.4	0.58	0.13	0.61	2.33
All	HOA	0.32	0.47	−0.68	0.75	1.85	0.77	0.5	−0.27	0.65	1.63
	OOA	0.72	0.43	−0.05	0.57	3.07	0.61	0.42	−0.12	0.56	3.02
	TOA	0.58	0.44	−0.20	0.57	4.3	0.64	0.46	−0.15	0.56	4.23

observed SOA concentrations, indicating the existence of missing SOA formation processes, e.g., aqueous-phase oxidation (Carlton et al., 2008; Washenfelder et al., 2011) and acid catalysis reactions of SOA from glyoxal (Liggio et al., 2005). The reported glyoxal imbalance between model simulations and observations can increase equivalent SOA mass by a few μg m^{-3} in urban areas, e.g., Mexico City (Volkamer et al., 2007). Furthermore, our models did not include other potential parent VOCs. For example, MBO, a potential parent VOC, has recently been reported as a possible source of SOA (H. Zhang et al., 2012a,b). Further investigation is needed to examine these missing processes through observations and improved models.

The simulated planetary boundary layer (PBL) and its related mixing processes can also cause a gap between model simulations and observations. Lin and McElroy (2010) showed that changing the PBL mixing scheme can reduce model biases over the United States by more than 10 ppb for surface ozone concentrations at night and by 2–5 ppb during the afternoon. However, computing the PBL height is difficult because the PBL height differs between algorithms approximately by a factor of 3 or 4, or more than 1 km (Seidel et al., 2010). More investigation is needed to calculate the appropriate PBL heights through improved observational methods and model schemes.

In this work, the VBS scheme accounts for the functionalization process. The recently proposed two-dimensional volatility basis set (2D-VBS) can simulate both functionalization and fragmentation processes (Donahue et al., 2011, 2012a,b; Murphy et al., 2012). However, a simplified functionalization scheme (analogous to the 1D-VBS approach used in this work) still showed a better performance than a functionalization and fragmentation scheme (Murphy et al., 2012), which requires too many parameterizations (e.g., functionalization kernel and functionalization/fragmentation branching ratio) that are poorly constrained.

4. Semi-volatile POA simulations

As discussed in Section 3.1, a significant overestimation of POA occurs in rural areas, possibly due to the absence of semi-volatile POA in the model. To examine the simulated sensitivity to semi-volatile POA, we conducted sensitivity model simulations using the VBS approach. We adopted an approach proposed by Robinson et al. (2007) even though their method possesses a high level of uncertainty, especially in the estimates of intermediate-volatility organic compounds (IVOCs) and semi-volatile organic compounds (SVOCs). In addition, it is computationally expensive. To resolve these issues, we suggest a simple approach to account for the semi-volatility of POA. The details are described below.

4.1. Semi-volatile POA simulation with the VBS approach

Based on the VBS approach, we added three more species with higher volatility, resulting in 9 volatility bins: $[C^*_i] = [0.01, 0.1, 1, 10, 100, 1000, 10{,}000, 100{,}000, 1{,}000{,}000]$ μg m^{-3}. The three highest volatility bins were used to represent IVOCs, and the others were used to represent SVOCs. The semi-volatile POA was partitioned into these volatility bins using normalized emission factors: [0.03, 0.06, 0.09, 0.14, 0.18, 0.30, 0.40, 0.50, 0.80]. The sum of these factors is 2.5. The semi-volatile POA emission amounts to 2.5 times the non-volatile POA emissions estimated from diesel emission profiles (Jathar et al., 2011; Robinson et al., 2007; Shrivastava et al., 2008; Tsimpidi et al., 2010). As a result, all POAs and SOAs were considered semi-volatile compounds.

We separated semi-volatile POA into fresh POA (emitted directly from the sources) and oxidized POA (oxidized with the hydroxyl radical). We assumed fresh POA to be HOA and oxidized POA to be OOA, as described by Shrivastava et al. (2008) and Murphy and Pandis (2009). The mass increase after one oxidation process is 7.5%, according to Robinson et al. (2007). For the aging of semi-volatile POA, we used an aging constant of 4×10^{-11} cm^3 $molecule^{-1}$ s^{-1}, which is the most widely used for semi-volatile POA aging (Bergstrom et al., 2012; Jathar et al., 2011; Murphy et al., 2011; Murphy and Pandis, 2010; Robinson et al., 2007; Shrivastava et al., 2008; Tsimpidi et al., 2010).

Table 6 summarizes the statistics from the comparison between the semi-volatile POA simulation and the AMS observations. Compared with the previous results shown in Tables 2 and 3, the model showed an improvement, especially for HOA concentrations. Specifically, the simulated high bias with non-volatile POA (RMSE of 3.11) was reduced after using semi-volatile POA (RMSE of 1.85). In general, the biases in the model were decreased. However, the remaining discrepancies between the model simulation and observations are highly region dependent. For example, the simulated HOA concentrations were higher than the observations in urban and urban downwind regions (Table 2) and are now lower than the observations (−75% and −72% for urban and urban-downwind regions, respectively), whereas the high bias in the rural regions (522%) is greatly reduced (−20%). The NMB of HOA in all regions is −68%, indicating that the fresh POA concentration is low, as semi-volatile POA aging reactions occur too rapidly. A smaller aging constant for semi-volatile POA may reduce this bias (i.e., more semi-volatile POA remains as fresh POA), even though the 4×10^{-11} cm^3 $molecule^{-1}$ s^{-1} aging constant was best for SOA.

In contrast, the low bias of the simulated OOA was greatly reduced in urban and urban downwind regions. However, the model slightly overestimates the observed OOA in rural regions.

These changes in simulated OOA concentrations are also consistent with those of HOA, indicating rapid semi-volatile POA aging reactions. The *R* values for all regions are slightly improved for HOA (0.47 from 0.43) and OOA (0.43 from 0.25). However, *R* is decreased slightly for TOA (0.44 from 0.47).

The consideration of semi-volatile POA did not result in a dramatic improvement in terms of TOA concentrations. However, including semi-volatile POA resulted in a significant improvement in both HOA and OOA concentrations, which is consistent with previous studies (Jathar et al., 2011; Robinson et al., 2007). As a result, the simulation with the semi-volatile POA better reproduced the observed HOA/OOA ratio.

4.2. Direct conversion of POA to SOA

Here, we suggest a simple approach that uses an additional POA (oxygenated POA) tracer to represent semi-volatile POA. Most chemical transport models employ two POA tracers: hydrophobic and hydrophilic POAs. Chemical oxidation and mixing with other soluble aerosols are important processes for changing the hydrophobicity of POA species. Thus, we considered more oxidation in the atmosphere. Therefore, hydrophilic POA is further oxidized to become oxygenated POA, which is analogous to SOA formed from semi-volatile POA, as discussed above. This conversion was simulated using an oxidation process by the OH radical with a rate constant of 4×10^{-11} cm^3 molecule^{-1} s^{-1} (the same value as in Section 4.1). Accompanying mass increases for each oxidation process were accounted for using different organic matter to organic carbon (OM/OC) ratios for each POA tracer. We applied different OM/OC ratios, i.e., 1.2 for hydrophobic, 1.8 for hydrophilic, and 2.4 for oxygenated POA, to maintain consistency with the study by Turpin and Lim (2001). They reported that the OM/OC ratios were 1.6 ± 0.2 for urban aerosols and 2.1 ± 0.2 for nonurban aerosols. In our model, the OM/OC ratio is close to 1.5 in nearby source regions and 2.4 in remote regions where most of the POA is oxidized. These OM/OC ratios are also within the range measured by Aiken et al. (2008).

The mass increases per one oxidation reaction were 50% (1.8/1.2) for hydrophobic to hydrophilic conversion and 33% (2.4/1.8) for hydrophilic to oxygenated conversion. These increases are comparable to the 50% mass increase suggested by Pye and Seinfeld (2010) and the 40% mass increase suggested by Grieshop et al. (2009). Note that the oxidation reaction occurs in the gas phase in other studies (Grieshop et al., 2009; Pye and Seinfeld, 2010; Robinson et al., 2007). However, this simple approach oxidizes aerosol tracers because it carries only aerosols.

As shown in Table 6, the results of the direct conversion are similar to the results reported in Section 4.1. The HOA concentrations in urban and urban-downwind regions are lower than the observations. However, the magnitude of the low bias was reduced (−42% for urban). The HOA concentrations in rural regions were higher (80%) than those of the observations, indicating that the conversion rate of fresh POA to oxygenated POA in the simple conversion case was lower than that in the case of semi-volatile POA with the VBS approach.

RMSEs greatly improved in all regions in terms of OOA and HOA. However, the simulated TOA results were slightly worse than the results of the non-volatile POA simulation. Similar to Section 4.1, the inclusion of semi-volatile POA improved the model performance in terms of HOA/OOA, but the performance of the model remained similar for TOA.

In the comparisons above, we demonstrated that the simple conversion approach can be as effective as the semi-volatile POA simulations suggested by Robinson et al. (2007), and sometimes even better, especially considering computational efficiency.

Table 7
Annual global OA budgets of the VBS approach with aging (4×10^{-11} cm^3 molecule^{-1} s^{-1}), the VBS approach with no aging and the two-product approach. We multiplied the carbon mass of POA by 2.1 to account for non-carbon mass. The burden of gas phase semi-volatiles is listed in parentheses. The net production rate is assumed equal to the deposition flux.

SOA scheme	4×10^{-11}	No aging	Two-product
Production [Tg yr^{-1}]			
- POA	47.8	47.8	47.8
- SOA	39.9	26.0	23.3
Burden [Tg]			
- POA	0.800	0.800	0.800
- SOA	1.159 (1.419)	0.889 (1.722)	0.908 (1.924)
$C^* = 10^{-2}$ μg m^{-3}	0.087 (0.001)		
$C^* = 10^{-1}$ μg m^{-3}	0.119 (0.004)		
$C^* = 10^{0}$ μg m^{-3}	0.332 (0.062)	0.222 (0.056)	
$C^* = 10^{1}$ μg m^{-3}	0.274 (0.190)	0.244 (0.208)	
$C^* = 10^{2}$ μg m^{-3}	0.186 (0.381)	0.216 (0.476)	
$C^* = 10^{3}$ μg m^{-3}	0.161 (0.781)	0.207 (0.982)	
Wet deposition [Tg yr^{-1}]			
- POA	39.4	39.4	39.4
- SOA	35.1	22.9	20.7
Dry deposition [Tg yr^{-1}]			
- POA	8.4	8.4	8.4
- SOA	4.8	3.0	2.6
Lifetime [s]			
- POA	6.6	6.6	6.6
- SOA	10.6	12.5	14.2

Although the consideration of semi-volatile POA in both methods did not produce significant improvements in terms of total OA predictions, it does show significant improvements in the HOA/OOA ratios. This is consistent with the results by Jathar et al. (2011) who showed that the simulated SOA to OA ratios were greatly increased and approached the observed ratios after including semi-volatile POA in the simulations.

5. Global budgets of OA species

We estimated the global budgets of OA species using three different models: our best model with the 4×10^{-11} cm^3 molecule^{-1} s^{-1} aging constant, the model with the VBS approach with no aging, and the model with the two-product method. The tabulated global source of SOA species using the two-product approach is 23.3 Tg yr^{-1}. Our estimates using the two-product approach here are also consistent with the 23–30.3 Tg yr^{-1} range reported in previous studies (Henze et al., 2008; Pye and Seinfeld, 2010).

Table 7 summarizes the simulated results of the OA budgets. Here, we focused mainly on values of the SOA species because the POA values are identical among the three models. A comparison between the VBS approach with no aging and the two-product scheme shows the effect of the updated yield parameters. A comparison between the model with aging (4×10^{-11} cm^3 molecule^{-1} s^{-1}) and with no aging shows the effect of chemical aging. We found that the model with aging yielded the highest total SOA production, i.e., 39.9 Tg yr^{-1}, which was 1.5 times higher than the 26.0 Tg yr^{-1} predicted by the no aging model. Moreover, the updated yield parameters resulted in relatively minor enhancements in SOA production relative to the two-product model (23.3 Tg yr^{-1}).

As expected from the comparison above, the SOA burden with aging (1.16 Tg) is 30% higher than that with no aging (0.89 Tg). However, this increase is substantially smaller than that for the production of SOA (53% increase) mainly because of the volatility distribution change in SOA. In comparison with the no aging case, the volatility distribution for the aging case shifts toward low saturation vapor pressure bins (Table 7). Therefore, the aerosol

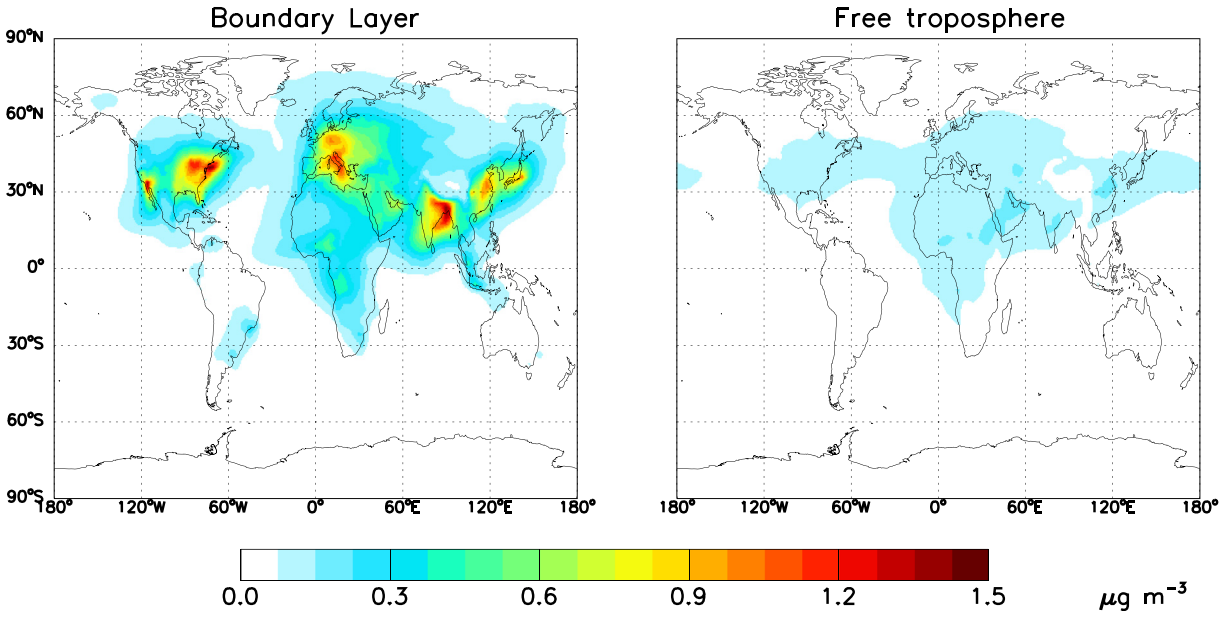

Fig. 6. The SOA increase between the VBS approach with aging (4×10^{-11} cm^3 molecule^{-1} s^{-1}) and with no aging case. The left panel shows the increase in the boundary layer (0–1 km) and the right panel shows the increase in the free troposphere (2–6.5 km).

phase is more favorable in the aging case. SOA from the model with aging is more concentrated in the boundary layer where vertical transport is very limited by wet deposition processes, especially in the form of aerosols. Consequently, the lifetime of SOA with aging (10.6 days) is shorter relative to that of SOA with no aging (12.5 days). Similarly, the SOA burden of the no aging case was slightly lower than that predicted using the two-product scheme although the SOA production of the no aging case was higher than that predicted using the two-product method.

Kanakidou et al. (2005) previously estimated 12–70 Tg yr^{-1} of SOA production based on global model simulations with no chemical aging of SOA. Farina et al. (2010) estimated 38.1 Tg yr^{-1} of global SOA production with chemical aging of SOA. Although our best estimate of global SOA production with the VBS approach (39.9 Tg yr^{-1}) is higher than that of the two-product scheme (23.3 Tg yr^{-1}), it is still lower than the top-down estimates of 50–380 Tg yr^{-1} by Spracklen et al. (2011), obtained using AMS observations and the GLOMAP global chemical transport model. Our best estimate of the global OA source using the VBS approach (87.7 Tg yr^{-1}) is also lower than the top-down estimate of 315 Tg yr^{-1} by Heald et al. (2010),[1] estimated based on satellite observations of aerosol optical depth. Our global SOA burden using the VBS approach is 1.16 Tg, higher than the 0.98 Tg given by Farina et al. (2010) and lower than the top-down estimate (1.84 Tg) of Spracklen et al. (2011). Finally, our OA burden is 1.96 Tg, slightly higher than the 1.7 Tg from the AeroCom multi-model mean (Textor et al., 2006) but lower than the 5.3 Tg estimated by Heald et al. (2010).[1] The lifetime of OA in our model is 8.2 days, which is within the range (4.3–11 days) of the AeroCom multi-model study (Textor et al., 2006) and slightly lower than the 9.4 days reported by Farina et al. (2010).

It has been reported that models underestimate SOA concentrations in the free troposphere as well as the boundary layer (Heald et al., 2005, 2011). To examine the effect of chemical aging on SOA in the free troposphere, we plotted the increased (aging minus no aging) SOA concentrations in the boundary layer and free troposphere in Fig. 6. Increases of SOA concentrations are spatially consistent with that of aromatic VOC emissions (Henze et al., 2008), reflecting only the chemical aging of anthropogenic SOA. In the boundary layer, the SOA concentrations increased to 1.50 μg m^{-3}, with a global mean increase of 0.10 μg m^{-3}. However, in the free troposphere, this increase was reduced with a global mean increase of 0.04 μg m^{-3} and a maximum increase of 0.20 μg m^{-3}. We found that the aerosol phase fraction of semi-volatiles in the aging case is 45%, much higher than that of semi-volatiles with no aging (34%). Due to limited upward transport by the accompanying wet scavenging with vertical updrafts, the SOA concentration increase owing to the chemical aging was reduced as altitude increased.

6. Effect of chemical aging on global DRF of SOA

We used our best estimate of SOA concentrations in Section 5 to compute the clear-sky DRF of SOA at the top of the atmosphere. We first computed the aerosol optical depths (AODs) at 19 spectral wavelength bands for the radiative transfer calculation using the MIE algorithm package (Wiscombe, 1980). A refractive index of 1.53–0.005i, an effective radius of 0.0212 μm, and a density of 1.8 g cm^{-3} were used for all OA species in this calculation (Chin et al., 2002). We used aerosol hygroscopic growth factors from Chin et al. (2002). Then, the calculated AODs at 19 wavelengths (ranging from 0.2 to 4.4 μm) were used in the National Center for Atmospheric Research Column Radiation Model version 2 (NCAR CRM2) for the DRF calculation. The meteorological input data needed for the computation were obtained from the GEOS-5 assimilated meteorological data.

The left panel of Fig. 7 shows the DRF of SOA for the no aging scenario. The spatial pattern of DRF reflects the aerosol concentrations; the highest DRF values occur in the Northern Hemisphere and in active biomass-burning regions. The area-weighted global mean value is −0.21 W m^{-2}, indicating the cooling effect on the Earth's climate.

The right panel of Fig. 7 shows the changes in DRF of SOA as a result of chemical aging reactions (i.e., DRF of SOA with aging minus that of SOA with no aging). Because the chemical aging adds to the SOA concentrations, the global mean DRF of SOA decreased to

[1] We applied an OM/OC ratio of 2.1 to convert TgC to Tg.

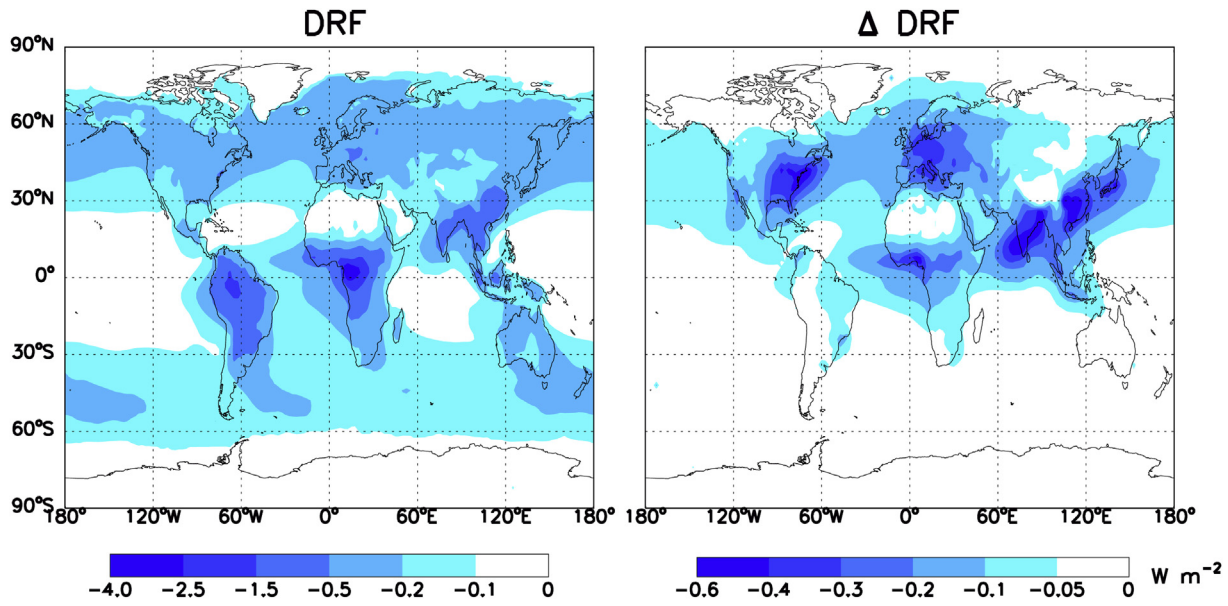

Fig. 7. Simulated clear-sky DRF of SOA with no aging (left) and decreased DRF of SOA after considering chemical aging (right) at the top of the atmosphere.

-0.28 W m^{-2}. The spatial pattern of DRF change is similar to Fig. 6. Notably, the global mean decrease in the SOA DRF because of chemical aging is -0.07 W m^{-2}, comparable to the AeroCom multi-model mean DRF of OA (-0.13 W m^{-2}) (Schulz et al., 2006). The AeroCom DRF was calculated based on the difference between pre-industrial and industrial OA concentrations, assuming that SOA is 100% biogenic. Therefore, the anthropogenic SOA DRF was assumed to be negligible in the AeroCom study and in the IPCC AR4 report (Forster et al., 2007). The DRF per burden in this study is -0.24 W m^{-2} Tg^{-1}, which is also consistent with that of the AeroCom study (mean value of -0.21 W m^{-2} Tg^{-1}, ranging from -0.39 W m^{-2} Tg^{-1} to -0.09 W m^{-2} Tg^{-1}). Therefore, there is a small possibility that our radiative transfer model overestimates the radiative effect of SOA.

The effect of chemical aging on the DRF of SOA is more important regionally, especially for industrialized regions, e.g., the eastern United States (-0.29 W m^{-2} over 100°W –70°W, 25°N –50°N), western Europe (-0.20 W m^{-2} over 10°W –50°E, 35°N –70°N), and East Asia (-0.17 W m^{-2} over 100°E –150°E, 10°N –50°N). These increased regional DRF values of SOA are 2.5–4 times higher than the globally increased mean DRF value, which has important implications for regional climates.

7. Conclusions

SOA is globally more dominant than POA. However, the SOA formation process and properties are still poorly understood. As a result, SOA models have typically significantly underestimated observations. Global SOA models using the two-product method have not yet considered the chemical aging of SOA, which many studies have shown to be important.

In this study, we implemented the VBS approach for SOA simulation in GEOS-Chem to simulate the chemical aging of SOA and examined its effects on the SOA burden and its climate implications. Using the model with different aging conditions, we conducted extensive evaluations of the model by comparison with observations in various regions (global, the United States, Europe, East Asia) and found that the model with the 4×10^{-11} cm^3 molecule^{-1} s^{-1} aging constant is most suitable for simulating SOA aging with the VBS approach. We also tested two semi-volatile POA simulations, i.e., the semi-volatile POA with the VBS approach and the simple conversion of POA to SOA. Both simulations showed improved results in terms of HOA and OOA but failed to improve the model results in terms of TOA.

We used our model results to analyze the effect of chemical aging on the global budgets of SOA. The inclusion of chemical aging increased the global SOA production by 53%, from 26.0 Tg yr^{-1} to 39.9 Tg yr^{-1}. Moreover, the global SOA burden was increased by 30%, from 0.89 Tg to 1.16 Tg. Chemical aging reduced the gap between the observation and the model and substantially increased the SOA production relative to previous studies. However, the model still underestimated the observations in urban regions and in the free troposphere, indicating possible missing sources. Further investigation of SOA formation (e.g., in-cloud processing) is needed through observations and improved models.

We computed the DRF of SOA species with aging and no aging conditions. The effect of chemical aging on the global mean SOA DRF was -0.07 W m^{-2}, comparable to the AeroCom multi-model mean OA DRF of -0.13 W m^{-2}. Because of its patch-like distribution, it is more important regionally, especially for industrialized regions. The DRF changes over the eastern United States, western Europe, and East Asia were 2.5–4 times higher than the global mean DRF change.

Acknowledgments

We thank two anonymous reviewers for their helpful comments on the manuscript. This study was funded by the Korea Meteorological Administration Research and Development Program under Grant CATER 2012-6121 and the National Research Foundation of Korea (NRF) grant funded by the Korean government (MISP) (2009-83527).

Appendix A. Supplementary data

Supplementary data related to this article can be found at http://dx.doi.org/10.1016/j.atmosenv.2013.08.055.

References

Aggarwal, S.G., Kawamura, K., 2009. Carbonaceous and inorganic composition in long-range transported aerosols over northern Japan: implication for aging of water-soluble organic fraction. Atmos. Environ. 43, 2532–2540.

Aiken, A., 2009. Mexico City aerosol analysis during MILAGRO using high resolution aerosol mass spectrometry at the urban supersite(T 0) – part 1: fine particle composition and organic source apportionment. Atmos. Chem. Phys. 9, 6633–6653.

Aiken, A.C., DeCarlo, P.F., Kroll, J.H., Worsnop, D.R., Huffman, J.A., Docherty, K.S., Ulbrich, I.M., Mohr, C., Kimmel, J.R., Sueper, D., 2008. O/C and OM/OC ratios of primary, secondary, and ambient organic aerosols with high-resolution time-of-flight aerosol mass spectrometry. Environ. Sci. Technol. 42, 4478–4485.

Batmunkh, T., Kim, Y., Lee, K., Cayetano, M., Jung, J., Kim, S., Kim, K., Lee, S., Kim, J., Chang, L., 2011. Time-resolved measurements of $PM_{2.5}$ carbonaceous aerosols at Gosan, Korea. J. Air Waste Manage. Assoc. 61, 1174–1182.

Bergstrom, R., der Gon, H.v., Prévôt, A., Yttri, K., Simpson, D., 2012. Modelling of organic aerosols over Europe (2002–2007) using a volatility basis set (VBS) framework: application of different assumptions regarding the formation of secondary organic aerosol. Atmos. Chem. Phys. 12, 8499–8527.

Bey, I., Jacob, D.J., Yantosca, R.M., Logan, J.A., 2001. Global modeling of tropospheric chemistry with assimilated meteorology – model description and evaluation. J Geophys. Res. 106, 073–023,095.

Birch, M., Cary, R., 1996. Elemental carbon-based method for monitoring occupational exposures to particulate diesel exhaust. Aerosol Sci. Technol. 25, 221–241.

Bond, T.C., Bhardwaj, E., Dong, R., Jogani, R., Jung, S., Roden, C., Streets, D.G., Trautmann, N.M., 2007. Historical emissions of black and organic carbon aerosol from energy-related combustion, 1850–2000. Glob. Biogeochem. Cycles 21.

Canagaratna, M., Jayne, J., Jimenez, J., Allan, J., Alfarra, M., Zhang, Q., Onasch, T., Drewnick, F., Coe, H., Middlebrook, A., 2007. Chemical and microphysical characterization of ambient aerosols with the aerodyne aerosol mass spectrometer. Mass Spectrom. Rev. 26, 185–222.

Carlton, A.G., Turpin, B.J., Altieri, K.E., Seitzinger, S.P., Mathur, R., Roselle, S.J., Weber, R.J., 2008. CMAQ model performance enhanced when in-cloud secondary organic aerosol is included: comparisons of organic carbon predictions with measurements. Environ. Sci. Technol. 42, 8798–8802.

Chin, M., Ginoux, P., Kinne, S., Torres, O., Holben, B.N., Duncan, B.N., Martin, R.V., Logan, J.A., Higurashi, A., Nakajima, T., 2002. Tropospheric aerosol optical thickness from the GOCART model and comparisons with satellite and sun photometer measurements. J. Atmos. Sci. 59, 461–483.

Cho, S.Y., Park, S.S., 2013. Resolving sources of water-soluble organic carbon in fine particulate matter measured at an urban site during winter. Environ. Sci. Process. Impacts 15, 524–534.

Choi, J.-K., Heo, J.-B., Ban, S.-J., Yi, S.-M., Zoh, K.-D., 2012. Chemical characteristics of $PM_{2.5}$ aerosol in Incheon, Korea. Atmos. Environ..

Chow, J.C., Watson, J.G., Pritchett, L.C., Pierson, W.R., Frazier, C.A., Purcell, R.G., 1993. The DRI thermal/optical reflectance carbon analysis system: description, evaluation and applications in US air quality studies. Atmos. Environ. 27, 1185–1201.

Chung, S., Seinfeld, J., 2002. Global distribution and climate forcing of carbonaceous aerosols. J. Geophys. Res. 107, 4407.

Cooke, W., Liousse, C., Cachier, H., Feichter, J., 1999. Construction of a 1×1 fossil fuel emission data set for carbonaceous aerosol and implementation and radiative impact in the ECHAM4 model. J. Geophys. Res. 104, 22122–22137, 22162.

Dommen, J., Metzger, A., Duplissy, J., Kalberer, M., Alfarra, M., Gascho, A., Weingartner, E., Prevot, A., Verheggen, B., Baltensperger, U., 2006. Laboratory observation of oligomers in the aerosol from isoprene/NO_x photooxidation. Geophys. Res. Lett. 33.

Donahue, N., Epstein, S., Pandis, S., Robinson, A., 2011. A two-dimensional volatility basis set: 1. organic-aerosol mixing thermodynamics. Atmos. Chem. Phys. 11, 3303–3318.

Donahue, N., Kroll, J., Pandis, S., Robinson, A., 2012a. A two-dimensional volatility basis set-part 2: diagnostics of organic-aerosol evolution. Atmos. Chem. Phys. 12, 615–634.

Donahue, N., Robinson, A., Stanier, C., Pandis, S., 2006. Coupled partitioning, dilution, and chemical aging of semivolatile organics. Environ. Sci. Technol. 40, 2635–2643.

Donahue, N.M., Henry, K.M., Mentel, T.F., Kiendler-Scharr, A., Spindler, C., Bohn, B., Brauers, T., Dorn, H.P., Fuchs, H., Tillmann, R., 2012b. Aging of biogenic secondary organic aerosol via gas-phase OH radical reactions. Proc. Natl. Acad. Sci. 109, 13503–13508.

Dzepina, K., Volkamer, R., Madronich, S., Tulet, P., Ulbrich, I., Zhang, Q., Cappa, C., Ziemann, P., Jimenez, J., 2009. Evaluation of recently-proposed secondary organic aerosol models for a case study in Mexico City. Atmos. Chem. Phys. 9, 5681–5709.

Eidels-Dubovoi, S., 2002. Aerosol impacts on visible light extinction in the atmosphere of Mexico City. Sci. Total Environ. 287, 213–220.

Farina, S.C., Adams, P.J., Pandis, S.N., 2010. Modeling global secondary organic aerosol formation and processing with the volatility basis set: implications for anthropogenic secondary organic aerosol. J. Geophys. Res. 115, D09202.

Feng, J., Hu, M., Chan, C.K., Lau, P., Fang, M., He, L., Tang, X., 2006. A comparative study of the organic matter in $PM_{2.5}$ from three Chinese megacities in three different climatic zones. Atmos. Environ. 40, 3983–3994.

Folinsbee, L.J., 1993. Human health effects of air pollution. Environ. Health Perspect. 100, 45.

Forster, P.V., Ramaswamy, P., Artaxo, T., Berntsen, R., Betts, D.W., Fahey, J., Haywood, J., Lean, D.C., Lowe, G., Myhre, J., Nganga, R., Prinn, G., Raga, M.S., Dorland, R.V., 2007. Changes in Atmospheric Constituents and in Radiative Forcing. Cambridge University Press, United Kingdom and New York, NY, USA.

Fountoukis, C., Nenes, A., 2007. ISORROPIA II: a computationally efficient thermodynamic equilibrium model for K^+–Ca^{2+}–Mg^{2+}–NH_4^+–Na^+–SO_4^{2-}–NO_3^-–Cl^-–H_2O aerosols. Atmos. Chem. Phys. Discuss. 7, 1893–1939.

Fu, T.M., Jacob, D.J., Wittrock, F., Burrows, J.P., Vrekoussis, M., Henze, D.K., 2008. Global budgets of atmospheric glyoxal and methylglyoxal, and implications for formation of secondary organic aerosols. J. Geophys. Res. 113.

Grieshop, A., Logue, J., Donahue, N., Robinson, A., 2009. Laboratory investigation of photochemical oxidation of organic aerosol from wood fires 1: measurement and simulation of organic aerosol evolution. Atmos. Chem. Phys. 9.

Griffin, R., Flagan, R., Seinfeld, J., 1999. Organic aerosol formation from the oxidation of biogenic hydrocarbons. J. Geophys. Res. 104, 3555–3567.

Guenther, A., Jiang, X., Heald, C., Sakulyanontvittaya, T., Duhl, T., Emmons, L., Wang, X., 2012. The model of emissions of gases and aerosols from nature version 2.1 (MEGAN2. 1): an extended and updated framework for modeling biogenic emissions. Geosci. Model Dev. 5, 1471–1492.

Hallquist, M., Wenger, J., Baltensperger, U., Rudich, Y., Simpson, D., Claeys, M., Dommen, J., Donahue, N., George, C., Goldstein, A., 2009. The formation, properties and impact of secondary organic aerosol: current and emerging issues. Atmos. Chem. Phys. 9, 5155.

Heald, C., Collett Jr., J., Lee, T., Benedict, K., Schwandner, F., Li, Y., Clarisse, L., Hurtmans, D., Van Damme, M., Clerbaux, C., 2012. Atmospheric ammonia and particulate inorganic nitrogen over the United States. Atmos. Chem. Phys. Discuss. 12, 19455–19498.

Heald, C., Jacob, D., Park, R., Russell, L., Huebert, B., Seinfeld, J., Liao, H., Weber, R., 2005. A large organic aerosol source in the free troposphere missing from current models. Geophys. Res. Lett. 32, L18809.

Heald, C.L., Coe, H., Jimenez, J.L., Weber, R.J., Bahreini, R., Middlebrook, A.M., Russell, L.M., Jolleys, M., Fu, T.M., Allan, J.D., Bower, K.N., Capes, G., Crosier, J., Morgan, W.T., Robinson, N.H., Williams, P.I., Cubison, M.J., DeCarlo, P.F., Dunlea, E.J., 2011. Exploring the vertical profile of atmospheric organic aerosol: comparing 17 aircraft field campaigns with a global model. Atmos. Chem. Phys. 11, 12673–12696.

Heald, C.L., Ridley, D.A., Kreidenweis, S.M., Drury, E.E., 2010. Satellite observations cap the atmospheric organic aerosol budget. Geophys. Res. Lett. 37.

Henze, D.K., Seinfeld, J.H., 2006. Global secondary organic aerosol from isoprene oxidation. Geophys. Res. Lett. 33, 09812.

Henze, D.K., Seinfeld, J.H., Ng, N.L., Kroll, J.H., Jacob, D.J., Heald, C.L., 2008. Global modeling of secondary organic aerosol formation from aromatic hydrocarbons: high-vs. low-yield pathways. Atmos. Chem. Phys..

Hirsch, R.M., Gilroy, E.J., 1984. Methods of fitting a straight line to data: examples in water resources. Water Resour. Bull. 20, 705–711.

Hudman, R.C., Jacob, D.J., Turquety, S., Leibensperger, E.M., Murray, L.T., Wu, S., Gilliland, A., Avery, M., Bertram, T.H., Brune, W., 2007. Surface and lightning sources of nitrogen oxides over the United States: magnitudes, chemical evolution, and outflow. J. Geophys. Res. 112, D12S05.

Jathar, S., Farina, S., Robinson, A., Adams, P., 2011. The influence of semi-volatile and reactive primary emissions on the abundance and properties of global organic aerosol. Atmos. Chem. Phys. Discuss. 11, 5493–5540.

Jeong, J., Park, R., Woo, J., Han, Y., Yi, S., 2010. Source contributions to carbonaceous aerosol concentrations in Korea. Atmos. Environ..

Jimenez, J., Canagaratna, M., Donahue, N., Prevot, A., Zhang, Q., Kroll, J., DeCarlo, P., Allan, J., Coe, H., Ng, N., 2009. Evolution of organic aerosols in the atmosphere. Science 326, 1525.

Kanakidou, M., Seinfeld, J., Pandis, S., Barnes, I., Dentener, F., Facchini, M., Van Dingenen, R., Ervens, B., Nenes, A., Nielsen, C., 2005. Organic aerosol and global climate modelling: a review. Atmos. Chem. Phys. 5, 1053–1123.

Kleindienst, T.E., Lewandowski, M., Offenberg, J.H., Jaoui, M., Edney, E.O., 2007. Ozone-isoprene reaction: re-examination of the formation of secondary organic aerosol. Geophys. Res. Lett. 34.

Kroll, J., Seinfeld, J., 2008. Chemistry of secondary organic aerosol: formation and evolution of low-volatility organics in the atmosphere. Atmos. Environ. 42, 3593–3624.

Kroll, J.H., Ng, N.L., Murphy, S.M., Flagan, R.C., Seinfeld, J.H., 2005. Secondary organic aerosol formation from isoprene photooxidation under high-NO_x conditions. Geophys. Res. Lett. 32, L18808.

Kroll, J.H., Ng, N.L., Murphy, S.M., Flagan, R.C., Seinfeld, J.H., 2006. Secondary organic aerosol formation from isoprene photooxidation. Environ. Sci. Technol. 40, 1869–1877.

Lane, T., Donahue, N., Pandis, S., 2008. Simulating secondary organic aerosol formation using the volatility basis-set approach in a chemical transport model. Atmos. Environ. 42, 7439–7451.

Lanz, V., Alfarra, M., Baltensperger, U., Buchmann, B., Hueglin, C., Prévôt, A., 2007. Source apportionment of submicron organic aerosols at an urban site by factor analytical modelling of aerosol mass spectra. Atmos. Chem. Phys. 7, 1503–1522.

Li, L., Wang, W., Feng, J., Zhang, D., Li, H., Gu, Z., Wang, B., Sheng, G., Fu, J., 2010. Composition, source, mass closure of $PM_{2.5}$ aerosols for four forests in eastern China. J. Environ. Sci. 22, 405–412.

Liao, H., Henze, D., Seinfeld, J., Wu, S., Mickley, L., 2007. Biogenic secondary organic aerosol over the United States: comparison of climatological simulations with observations. J. Geophys. Res. 112, D06201.

Liggio, J., Li, S.M., McLaren, R., 2005. Reactive uptake of glyoxal by particulate matter. J. Geophys. Res. 110.

Lin, J.-T., McElroy, M.B., 2010. Impacts of boundary layer mixing on pollutant vertical profiles in the lower troposphere: implications to satellite remote sensing. Atmos. Environ. 44, 1726–1739.

Liu, H., Jacob, D.J., Bey, I., Yantosca, R.M., 2001. Constraints from 210Pb and 7Be on wet deposition and transport in a global three-dimensional chemical tracer

model driven by assimilated meteorological fields. J. Geophys. Res. 106, 12109–12128.
Liu, Z., Wang, Y., Vrekoussis, M., Richter, A., Wittrock, F., Burrows, J.P., Shao, M., Chang, C.C., Liu, S.C., Wang, H., 2012. Exploring the missing source of glyoxal (CHOCHO) over China. Geophys. Res. Lett. 39.
Malm, W.C., Sisler, J.F., Huffman, D., Eldred, R.A., Cahill, T.A., 1994. Spatial and seasonal trends in particle concentration and optical extinction in the United States. J. Geophys. Res. 99, 1347–1370.
Mari, C., Jacob, D.J., Bechtold, P., 2000. Transport and scavenging of soluble gases in a deep convective cloud. J. Geophys. Res. 105, 22222–22255, 22267.
Ming, Y., Ramaswamy, V., Ginoux, P.A., Horowitz, L.H., 2005. Direct radiative forcing of anthropogenic organic aerosol. J. Geophys. Res. 110.
Miyazaki, Y., Kondo, Y., Han, S., Koike, M., Kodama, D., Komazaki, Y., Tanimoto, H., Matsueda, H., 2007. Chemical characteristics of water-soluble organic carbon in the Asian outflow. J. Geophys. Res. 112.
Mu, M., Randerson, J., van der Werf, G., Giglio, L., Kasibhatla, P., Morton, D., Collatz, G., DeFries, R., Hyer, E., Prins, E., 2011. Daily and 3-hourly variability in global fire emissions and consequences for atmospheric model predictions of carbon monoxide. J. Geophys. Res. 116, 24303.
Murphy, B., Donahue, N., Fountoukis, C., Dall'Osto, M., O'Dowd, C., Kiendler-Scharr, A., Pandis, S., 2012. Functionalization and fragmentation during ambient organic aerosol aging: application of the 2-D volatility basis set to field studies. Atmos. Chem. Phys. 12, 10797–10816.
Murphy, B., Donahue, N., Fountoukis, C., Pandis, S., 2011. Simulating the oxygen content of ambient organic aerosol with the 2D volatility basis set. Atmos. Chem. Phys. 11, 7859–7873.
Murphy, B.N., Pandis, S.N., 2009. Simulating the formation of semivolatile primary and secondary organic aerosol in a regional chemical transport model. Environ. Sci. Technol. 43, 4722–4728.
Murphy, B.N., Pandis, S.N., 2010. Exploring summertime organic aerosol formation in the eastern United States using a regional-scale budget approach and ambient measurements. J. Geophys. Res. 115.
Myhre, G., Berglen, T., Johnsrud, M., Hoyle, C., Berntsen, T., Christopher, S., Fahey, D., Isaksen, I., Jones, T., Kahn, R., 2009. Modelled radiative forcing of the direct aerosol effect with multi-observation evaluation. Atmos. Chem. Phys. 9, 1365–1392.
Ng, N.L., Kroll, J.H., Keywood, M.D., Bahreini, R., Varutbangkul, V., Flagan, R.C., Seinfeld, J.H., Lee, A., Goldstein, A.H., 2006. Contribution of first-versus second-generation products to secondary organic aerosols formed in the oxidation of biogenic hydrocarbons. Environ. Sci. Technol. 40, 2283–2297.
Odum, J., Hoffmann, T., Bowman, F., Collins, D., Flagan, R., Seinfeld, J., 1996. Gas/particle partitioning and secondary organic aerosol yields. Environ. Sci. Technol. 30, 2580–2585.
Pankow, J., 1994a. An absorption model of gas/particle partitioning of organic compounds in the atmosphere. Atmos. Environ. 28, 185–188.
Pankow, J.F., 1994b. An absorption model of the gas/aerosol partitioning involved in the formation of secondary organic aerosol. Atmos. Environ. 28, 189–193.
Park, R.J., Jacob, D.J., Chin, M., Martin, R.V., 2003. Sources of carbonaceous aerosols over the United States and implications for natural visibility. J. Geophys. Res. 108, 4355.
Park, R.J., Jacob, D.J., Field, B.D., Yantosca, R.M., Chin, M., 2004. Natural and transboundary pollution influences on sulfate-nitrate-ammonium aerosols in the United States: implications for policy. J. Geophys. Res. 109, D15204.
Park, R.J., Jacob, D.J., Kumar, N., Yantosca, R.M., 2006. Regional visibility statistics in the United States: natural and transboundary pollution influences, and implications for the Regional Haze Rule. Atmospheric Environment 40, 5405–5423.
Pathak, R.K., Wang, T., Ho, K., Lee, S., 2011. Characteristics of summertime $PM_{2.5}$ organic and elemental carbon in four major Chinese cities: implications of high acidity for water-soluble organic carbon (WSOC). Atmos. Environ. 45, 318–325.
Pavia, D., Thomson, M.L., Clarke, S.W., Shannon, H.S., 1977. Effect of lung function and mode of inhalation on penetration of aerosol into the human lung. Thorax 32, 194.
Pavuluri, C.M., Kawamura, K., Uchida, M., Kondo, M., Fu, P., 2013. Enhanced modern carbon and biogenic organic tracers in Northeast Asian aerosols during spring/summer. J. Geophys. Res. Atmos..
Pye, H., Chan, A., Barkley, M., Seinfeld, J., 2010. Global modeling of organic aerosol: the importance of reactive nitrogen (NO_x and NO_3). Atmos. Chem. Phys. 10, 11261–11276.
Pye, H., Seinfeld, J., 2010. A global perspective on aerosol from low-volatility organic compounds. Atmos. Chem. Phys. 10, 4377–4401.
Pye, H.O.T., Liao, H., Wu, S., Mickley, L.J., Jacob, D.J., Henze, D.J., Seinfeld, J.H., 2009. Effect of changes in climate and emissions on future sulfate-nitrate-ammonium aerosol levels in the United States. J. Geophys. Res. 114.
Robinson, A., Donahue, N., Shrivastava, M., Weitkamp, E., Sage, A., Grieshop, A., Lane, T., Pierce, J., Pandis, S., 2007. Rethinking organic aerosols: semivolatile emissions and photochemical aging. Science 315, 1259.
Schulz, M., Textor, C., Kinne, S., Balkanski, Y., Bauer, S., Berntsen, T., Berglen, T., Boucher, O., Dentener, F., Guibert, S., 2006. Radiative forcing by aerosols as derived from the AeroCom present-day and pre-industrial simulations. Atmos. Chem. Phys. 6, 5246.
Seidel, D.J., Ao, C.O., Li, K., 2010. Estimating climatological planetary boundary layer heights from radiosonde observations: comparison of methods and uncertainty analysis. J. Geophys. Res. 115.
Shrivastava, M.K., Lane, T.E., Donahue, N.M., Pandis, S.N., Robinson, A.L., 2008. Effects of gas particle partitioning and aging of primary emissions on urban and regional organic aerosol concentrations. J. Geophys. Res. 113, D18301.
Spracklen, D.V., Jimenez, J.L., Carslaw, K.S., Worsnop, D.R., Evans, M.J., Mann, G.W., Zhang, Q., Canagaratna, M.R., Allan, J., Coe, H., McFiggans, G., Rap, A., Forster, P., 2011. Aerosol mass spectrometer constraint on the global secondary organic aerosol budget. Atmos. Chem. Phys. 11, 12109–12136.
Sullivan, A., Peltier, R., Brock, C., De Gouw, J., Holloway, J., Warneke, C., Wollny, A., Weber, R., 2006. Airborne measurements of carbonaceous aerosol soluble in water over northeastern United States: method development and an investigation into water- soluble organic carbon sources. J. Geophys. Res. 111.
Sullivan, A., Weber, R., Clements, A., Turner, J., Bae, M., Schauer, J., 2004. A method for on-line measurement of water-soluble organic carbon in ambient aerosol particles: results from an urban site. Geophys. Res. Lett. 31, L13105.
Textor, C., Schulz, M., Guibert, S., Kinne, S., Balkanski, Y., Bauer, S., Berntsen, T., Berglen, T., Boucher, O., Chin16, M., 2006. Analysis and quantification of the diversities of aerosol life cycles within AeroCom. Atmos. Chem. Phys. 6, 1777–1813.
Tsimpidi, A., Karydis, V., Zavala, M., Lei, W., Molina, L., Ulbrich, I., Jimenez, J., Pandis, S., 2010. Evaluation of the volatility basis-set approach for the simulation of organic aerosol formation in the Mexico City metropolitan area. Atmos. Chem. Phys. 10, 525–546.
Turpin, B.J., Lim, H.J., 2001. Species contributions to $PM_{2.5}$ mass concentrations: revisiting common assumptions for estimating organic mass. Aerosol Sci. Technol. 35, 602–610.
van der Werf, G., Randerson, J., Giglio, L., Collatz, G., Mu, M., Kasibhatla, P., Morton, D., DeFries, R., Jin, Y., van Leeuwen, T., 2010. Global fire emissions and the contribution of deforestation, savanna, forest, agricultural, and peat fires (1997–2009). Atmos. Chem. Phys. 10, 11707–11735.
Volkamer, R., Jimenez, J.L., San Martini, F., Dzepina, K., Zhang, Q., Salcedo, D., Molina, L.T., Worsnop, D.R., Molina, M.J., 2006. Secondary organic aerosol formation from anthropogenic air pollution: rapid and higher than expected. Geophys. Res. Lett. 33, 17.
Volkamer, R., San Martini, F., Molina, L.T., Salcedo, D., Jimenez, J.L., Molina, M.J., 2007. A missing sink for gas-phase glyoxal in Mexico City: formation of secondary organic aerosol. Geophys. Res. Lett. 34.
Wang, Y., Jacob, D.J., Logan, J.A., 1998. Global simulation of tropospheric O_3-NO_x-hydrocarbon chemistry 1. Model formulation. J. Geophys. Res. 103, 10710–10713, 10725.
Washenfelder, R., Young, C., Brown, S., Angevine, W., Atlas, E., Blake, D., Bon, D., Cubison, M., De Gouw, J., Dusanter, S., 2011. The glyoxal budget and its contribution to organic aerosol for Los Angeles, California, during CalNex 2010. J. Geophys. Res. 116.
Weber, R.J., Sullivan, A.P., Peltier, R.E., Russell, A., Yan, B., Zheng, M., de Gouw, J., Warneke, C., Brock, C., Holloway, J.S., 2007. A study of secondary organic aerosol formation in the anthropogenic-influenced southeastern United States. J. Geophys. Res. 112, D13302.
Wiscombe, W.J., 1980. Improved Mie scattering algorithms. Appl. Opt. 19, 1505–1509.
Yttri, K., Aas, W., Bjerke, A., Ceburnis, D., Dye, C., Emblico, L., Facchini, M., Forster, C., Hanssen, J., Hansson, H., 2007. Elemental and organic carbon in PM_{10}: a one year measurement campaign within the European Monitoring and Evaluation Programme EMEP. Atmos. Chem. Phys. Discuss. 7, 3859–3899.
Yu, F., 2011. A secondary organic aerosol formation model considering successive oxidation aging and kinetic condensation of organic compounds: global scale implications. Atmos. Chem. Phys. 11, 1083–1099.
Zhang, F., Xu, L., Chen, J., Yu, Y., Niu, Z., Yin, L., 2012a. Chemical compositions and extinction coefficients of $PM_{2.5}$ in peri-urban of Xiamen, China, during June 2009–May 2010. Atmos. Res. 106, 150–158.
Zhang, H., Worton, D.R., Lewandowski, M., Ortega, J., Rubitschun, C.L., Park, J.-H., Kristensen, K., Campuzano-Jost, P., Day, D.A., Jimenez, J.L., 2012b. Organosulfates as tracers for secondary organic aerosol (SOA) formation from 2-methyl-3-buten-2-ol (MBO) in the atmosphere. Environ. Sci. Technol. 46, 9437–9446.
Zhang, Q., Jimenez, J., Canagaratna, M., Allan, J., Coe, H., Ulbrich, I., Alfarra, M., Takami, A., Middlebrook, A., Sun, Y., 2007. Ubiquity and dominance of oxygenated species in organic aerosols in anthropogenically-influenced Northern Hemisphere midlatitudes. Geophys. Res. Lett. 34, L13801.
Zhang, Q., Worsnop, D., Canagaratna, M., Jimenez, J.L., 2005. Hydrocarbon-like and oxygenated organic aerosols in Pittsburgh: insights into sources and processes of organic aerosols. Atmos. Chem. Phys. Discuss. 5, 8421–8471.
Zhao, P., Dong, F., He, D., Zhao, X., Zhang, X., Zhang, W., Yao, Q., Liu, H., 2013. Characteristics of concentrations and chemical compositions for $PM_{2.5}$ in the region of Beijing, Tianjin, and Hebei, China. Atmos. Chem. Phys. 13, 4631–4644.